Plasma Physics and Controlled Fusion

Check for updates

OPEN ACCESS

RECEIVED
23 December 2025

REVISED
22 May 2026

ACCEPTED FOR PUBLICATION
10 August 2026

PUBLISHED
21 August 2026

PAPER

Development of a high-current, high fusion performance scenario on JET: physics insights and operational challenges

L Garzotti[1,*], D Frigione[2], P Lomas[1], F Rimini[1], D Van Eester[3], V K Zotta[4], S Aleiferis[5], E Alessi[6], F Auriemma[7], R B Morales[1], I S Carvalho[8], P Carvalho[9], A Chomiczewska[10], R Cicioni[11], E De La Luna[12], D R Ferreira[9], A Field[1], M Fontana[13], L Frassinetti[14], S Gabriellini[1], Z Ghani[1], E Giovannozzi[15], C Giroud[1], W Gromelski[10], N Grzybicka[10], I Ivanova Stanik[10], V Kiptily[1], K Kirov[1], M Lennholm[1], C Leoni[4], J Lombardo[7], C Lowry[1], C F Maggi[1], J Mailloux[1], S Menmuir[1], S Nowak[6], V Parail[1], A Patel[1], A Pau[16], E Peluso[2,15], C Perez von Thun[10], L Piron[11], G Pucella[15], C Reux[17], S Saarelma[1], O Sauter[16], E Solano[12], C Sozzi[6], Ž. Štancar[1], C Stuart[1], H Sun[1], G Telesca[10], D Tskhakaya[18], M Valovič[1], N Wendler[10], JET Contributors[19] and the EUROfusion Tokamak Exploitation Team[20]

1 Culham Campus, Abingdon, Northern, Ireland
2 Università di Roma Tor Vergata, Via del Politecnico 1, Roma, Italy
3 Laboratory for Plasma Physics LPP-ERM/KMS, B-1000 Brussels, Belgium
4 Dipartimento di Ingegneria Astronautica, Elettrica ed Energetica, SAPIENZA Università di Roma, Via Eudossiana 18, 00184 Roma, Italy
5 School of Applied Mathematical and Physical Science, National Technical University of Athens, 15780 Athens, Greece
6 Institute for Plasma Science and Technology, CNR, via R. Cozzi 53, 20125 Milano, Italy
7 Consorzio RFX (CNR, ENEA, INFN, Università di Padova, Acciaierie Venete SpA), C.so Stati Uniti 4, 35127 Padova, Italy
8 ITER Organization, Route de Vinon-sur-Verdon, CS 90 046, 13067 Saint Paul, Lez Durance Cedex, France
9 Instituto de Plasmas e Fusão Nuclear, Instituto Superior Técnico, Universidade de Lisboa, 1049-001 Lisboa, Portugal
10 Institute of Plasma Physics and Laser Microfusion, Hery 23, 01-497 Warsaw, Poland
11 Dipartimento di Fisica 'G. Galilei', Università degli Studi di Padova, Padova, Italy
12 Laboratorio Nacional de Fusión, CIEMAT, Madrid, Spain
13 Tokamak Energy Ltd, Milton Park, Oxfordshire, Milton Park, OX14 4SD, United Kingdom
14 Fusion Plasma Physics, EECS, KTH Royal Institute of Technology, Stockholm, SE-10044, Sweden
15 ENEA, Nuclear Department, C.R. ENEA-Frascati, Via E. Fermi 45, 00044 Frascati, RM, Italy
16 Ecole Polytechnique Fédérale de Lausanne (EPFL), Swiss Plasma Center (SPC), CH-1015 Lausanne, Switzerland
17 CEA, IRFM, F-13108 Saint Paul, Lez Durance, France
18 Institute of Plasma Physics of the CAS, Za Slovankou 1782/3, 182 00 Praha 8, Czech Republic
19 See the author list of *Overview of T and D-T results in JET with ITER-like wall* by C F Maggi *et al* Nuclear Fusion Special Issue: Overview and Summary Papers from the 29th Fusion Energy Conference (London, UK, 16–21 2023)
20 See the author list of *Overview of the EUROfusion Tokamak Exploitation programme in support of ITER and DEMO* by E Joffrin *et al* Nuclear Fusion Special Issue: Overview and Summary Papers from the 29th Fusion Energy Conference (London, UK, 16–21 2023)
* Author to whom any correspondence should be addressed.

E-mail: luca.garzotti@ukaea.uk

Keywords: tokamaks, deuterium–tritium, plasma scenarios

Abstract

Since the installation of a beryllium–tungsten (Be/W) first wall on JET an intense scenario development programme has taken place to realize a high-current (3.5–4 MA) scenario, denominated JET baseline scenario, with $q_{95} \sim 3$, $\beta_N \sim 1.8$ and capable of delivering high fusion performance ($P_{fus} > 10$ MW) for 5 s in the deuterium–tritium (D–T) campaigns conducted in 2021 and 2023. The JET baseline scenario was realized in D–T at 3.5 MA in 2021 (DTE2 campaign), but, despite achieving transitorily $P_{fus} \sim 8$ MW, it could not be sustained for more than 3 s. In this paper we will revisit and expand the analysis of the baseline scenario at 3.5 MA and present new results obtained in D–T at 3.0 MA in DTE3, where we were able to sustain the scenario for 5 s. We will also present recent modelling results showing how available semi-empirical and first-principles transport models can explain a variety of phenomena ranging from fusion performance, impurity transport and control of the fuelling mix. Many of these points are potentially relevant for bigger machines such as ITER. Finally, we will discuss open questions and improvements to our present modelling capabilities required to extrapolate the results to power plant devices.

1. Introduction

To obtain good confinement of the alpha particles generated by the fusion reactions and necessary for the main heating of the plasma, next-generation tokamaks operating in deuterium–tritium (D–T) and aiming at fusion performance with $Q \approx 10$ (Q being the ratio between fusion power produced by the plasma and auxiliary heating power injected in the plasma), will feature plasma current I_p in the order of several MA. For example, in scenarios aiming at obtaining $Q = 10$, ITER will operate at $I_p = 15$ MA [1] and SPARC at $I_p = 8.7$ MA [2].

In this context, being the largest operational tokamak in the world, JET is a unique device to explore the high plasma current regime ahead of D–T operation on larger tokamaks in the future. In fact, JET is the only tokamak in the world capable of D–T operation and, in principle, of plasma current in excess of 4 MA, meaning that JET high-current plasmas are the closest to ITER operating conditions, at least as far as core plasma parameters are concerned.

In addition, since 2011, JET has been equipped with a beryllium (Be) wall and tungsten (W) divertor to reduce the T retention observed in presence of the previous carbon (C) wall and deemed unacceptable for a reactor. This makes JET even more relevant, since it can operate with reactor-like plasma facing components and address the challenges associated with operations with a metallic wall and divertor.

Between 2021 and 2023, the JET DTE2 and DTE3 experimental campaigns featured operations with D–T plasma composition aiming, amongst other things, at recovering the confinement properties and the fusion performance obtained with a C wall in the previous DTE1 campaign in 1997 and sustain them for 5 s [3, 4]. To this purpose, two main operational scenarios were developed successively in D, T and D–T: the high-current JET baseline scenario ($I_p \geqslant 3.5$ MA, $q_{95} \approx 3$ and $\beta_N \approx 1.8$) [5] and the JET hybrid scenario ($I_p \leqslant 3$ MA, $q_{95} \approx 4.8$ and $\beta_N \geqslant 2$) [6].

In this paper we concentrate on the JET baseline scenario, which was developed at 3.5 MA in D with the potential of generating a fusion power of $\approx$10 MW in D–T, but could not be sustained for 5 s. In particular, we present further analysis of the baseline scenario at 3.5 MA obtained in DTE2, describe the modifications we implemented to sustain it for 5 s in DTE3, analyse the results in terms of confinement and fusion performance and consider the lessons learnt from the development of a high-current scenario for D–T in a metal wall machine.

Analysis and modelling following the DTE2 campaign showed that two main factors prevented the JET baseline scenario from being sustained for 5 s at 3.5 MA: the improved particle confinement in D–T resulted in higher densities for the same plasma current leading to higher levels of radiated power and lower margin above the L–H threshold with respect to D, and the compound ELM activity necessary to flush the W was more difficult to induce in D–T for the same gas throughput as in D.

The results of the analysis suggested running the scenario at 3.0 MA and with increased fuelling to sustain it for 5 s with less concern for the fusion performance. These modifications allowed to run the scenario for 5 s until the programmed end of the pulse. The 5 s 3.0 MA baseline plasma produced 18 MJ of fusion energy over 5 s with $\sim$30 MW of additional power, a modest performance compared to the record fusion power obtained in DTE2, but provided valuable insight into critical aspects of operation at high current in a W environment such as margin above L–H threshold, W transport in the plasma core, pedestal and SOL and details of the heat and particle sources.

The structure of the paper is the following: in section 2 we discuss briefly the prerequisites and the implications of operating at high plasma current; in section 3 we review the results obtained at 3.5 MA in DTE2 and discuss why the JET baseline scenario was not sustained in D–T at this plasma current; in section 4 we present the results obtained at 3.0 MA in DTE3, where the scenario was sustained for 5 s, and in section 5 we list the lessons learnt during the scenario development activity on JET and we draw some conclusions.

2. High current operation at JET

In order to appreciate the extent and the relevance of high-current operation on JET, we consider every JET pulse for which the plasma current was measured, we take its maximum value for every pulse and discard values $\leqslant$1 MA to exclude dry-runs and pulses where the break-down was not sustained.

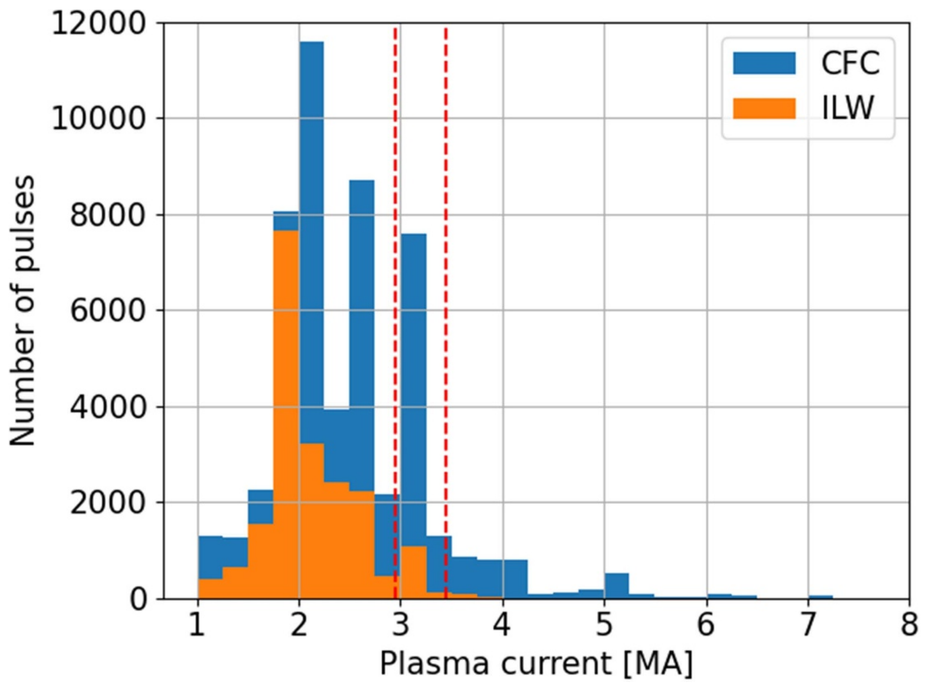

Figure 1. Distribution of all JET plasma pulses as function of plasma current separated according to first wall material. Blue (CFC): carbon wall; orange (ILW): beryllium and tungsten ITER-like wall.

The distribution is shown in figure 1 both for plasmas with C and Be/W wall, and indicates that, in the case of C wall, only 25.5% of JET pulses features $I_\mathrm{p} \geqslant 2.95$ MA and 7.7% of the pulses features $I_\mathrm{p} \geqslant 3.45$ MA. Repeating the analysis for the Be/W wall gives 7% of the pulses with $I_\mathrm{p} \geqslant 2.95$ MA and 0.8% of the pulses with $I_\mathrm{p} \geqslant 3.45$ MA.

The information on the high current regime is concentrated in a relatively small number of pulses because of their operational requirements and implications. In fact, to realize high-current, high-performance plasmas on JET all systems such as central solenoid, toroidal field coils, NBI and ICRH heating, and, as will be explained later, pellet injector need to be working simultaneously at the upper limits of their operational range. In particular, to operate high fusion performance plasmas on JET with $I_\mathrm{p} \geqslant 3.5$ MA the maximum additional heating power ($P_\mathrm{NBI} + P_\mathrm{ICRH} \approx 37$ MW) has to be reliably available.

The main risk associated with the failure of one of the above mentioned systems is a plasma disruption. Figure 2 shows the disruption force as function of the plasma current, indicating that, for $I_\mathrm{p} \geqslant 3.5$ MA, it can exceed 400 and even approach 500 tonnes. At this level there is a significant danger of damaging the vacuum vessel or the in-vessel components. In addition, as reported in [7], in a Be/W machine, disruption forces are higher than in a C machine and disruption mitigation strategies become mandatory. On JET massive injection of a mixture of 10% Ar and 90% D (or H) obtained by means of a disruption mitigation valve was used in case of disruption at $I_\mathrm{p} \geqslant 2.0$ MA or total plasma stored energy (thermal plus magnetic) $W_\mathrm{tot} \geqslant 5$ MJ [8].

The disruptivity of JET baseline plasmas in D at $I_\mathrm{p} \geqslant 3.5$ MA is $\approx 50\%$ mainly due to unplanned losses of auxiliary heating power (especially NBI) or sudden ingress in the plasma of W coming from the divertor. Therefore, high current plasmas were treated as a scarce resource and ran with caution only when the probability of success was the highest.

3. JET baseline scenario at 3.5 MA

Immediately after the installation of the Be/W wall, the development of the high current JET baseline scenario was started with the aim of recovering the performance obtained with the C wall and followed a staged approach described in [5]. To illustrate the progress towards recovering the performance achieved on JET with the C wall in the same way as in [9], figure 3 shows the experimental plasma stored energy as function of the estimate of the same quantity based on the $H_{98(y,2)}$ confinement scaling

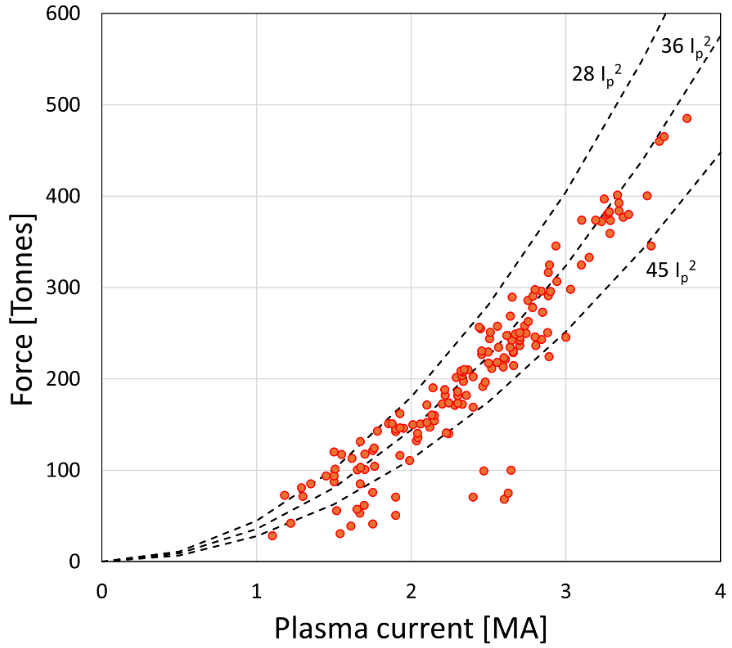

Figure 2. Disruption vertical vessel forces for the JET tokamak as function of the plasma current. The dashed lines correspond to three quadratic fits of the trend.

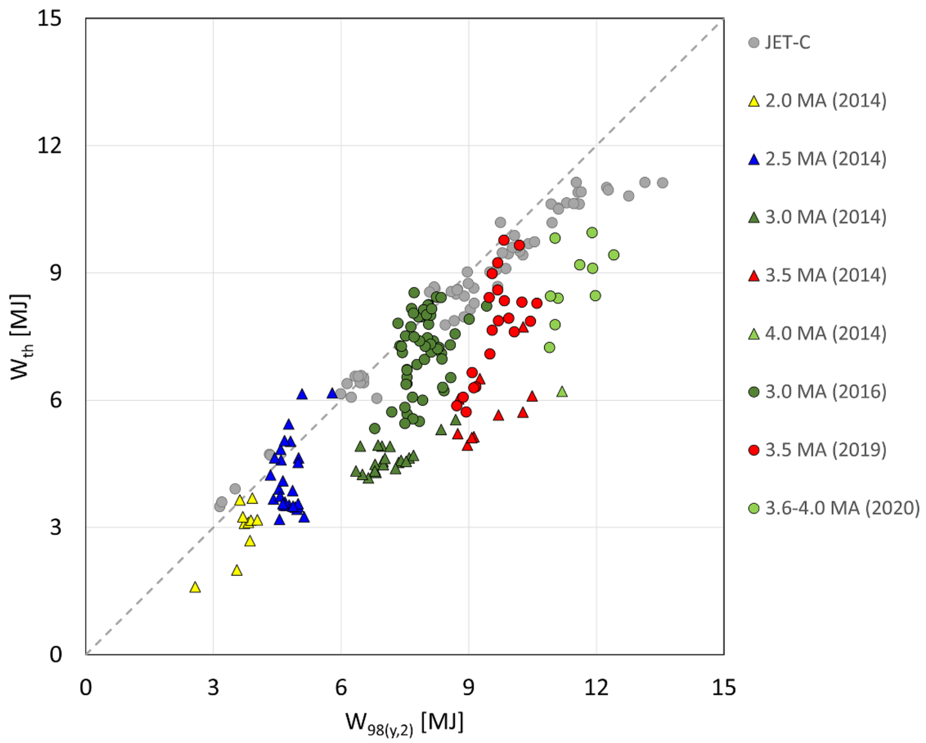

Figure 3. Measured plasma stored energy versus values estimated from the $H_{98(y,2)}$ scaling law. Colour triangles are pre-2014 data and colour circles are data between 2016 and 2021 showing the recovery of the confinement obtained with the CFC wall (grey circles) thanks to the optimization of the fuelling recipe with the Be/W wall.

law. It can be seen that, until 2014, lower stored energy (an therefore lower energy confinement) than with the C wall was observed for $I_p > 2.5$ MA.

In 2016, stored energy comparable to the C wall was obtained at 3.5 MA thanks to an optimization process of the plasma fuelling and pumping scheme. In particular, low gas dosing from the main chamber resulted in improved pedestal and core confinement and injection of ELM pacing pellets promoted the ELM activity necessary for impurity flushing [10] and density control. Moreover, the change

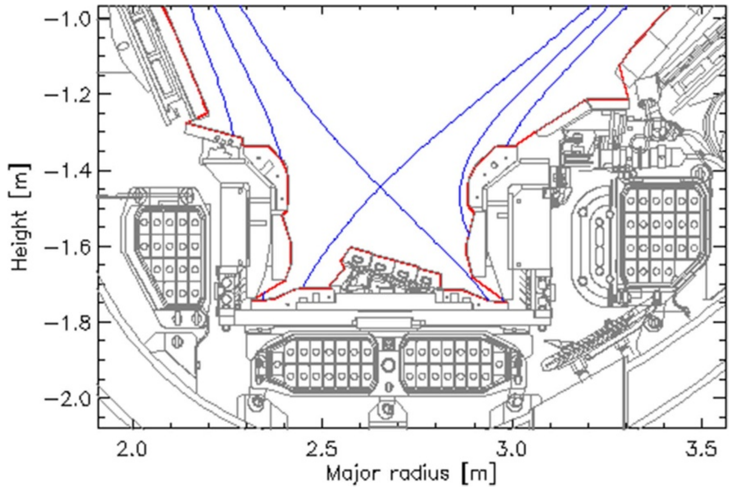

Figure 4. Divertor configuration for the JET baseline scenario (JPN 96893 at $t = 10$ s) showing the proximity of the inner and outer strike-points to the pump duct. The strike-point position was swept with an amplitude of 4 cm at 4 Hz to avoid overheating the divertor tiles. D gas was introduced from the top of the main vacuum chamber.

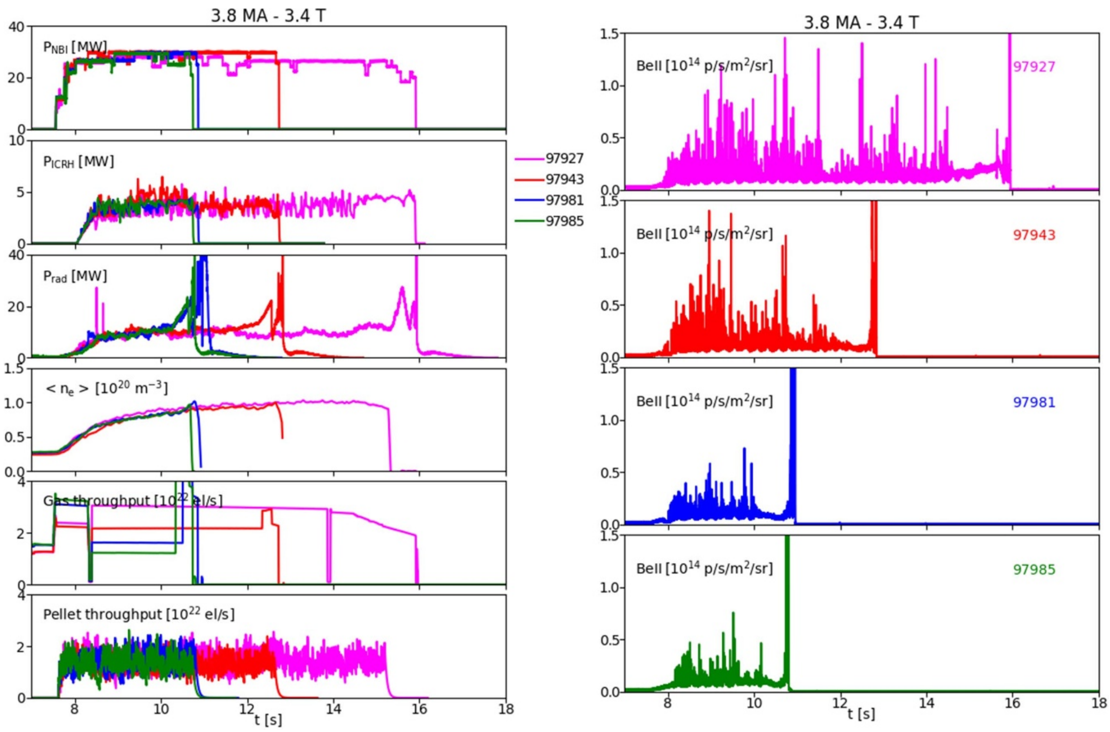

Figure 5. Left: plasma parameters for a series of pulses with decreasing gas particle throughput. Right: BeII emission representing ELM activity and showing that it ceases earlier and earlier with decreasing gas fuelling rate. Only the pulses with gas fuelling rate $>2 \times 10^{22}$ el/s could be sustained for 5 s.

of divertor geometry from horizontal to corner target configuration maximized the pumping by bringing the strike points closer to the pumping ducts, as shown in figure 4, and contributed to minimizing the plasma density at the separatrix, n_{sep}, reducing the pedestal transport in H-mode as observed experimentally and, for type-I ELM plasmas, interpreted in the light of MHD stability and kinetic profile analysis [11]. In 2019, the successful fuelling and pumping recipe was extended to 3.5 MA, and showed clear improvement at 3.6–4 MA.

In order to understand the role of the fuelling in determining the plasma behaviour and the stationarity of the pulse, we analysed a fuelling scan for a D plasma at 3.8 MA / 3.4 T. The results are shown in figure 5 where it can be seen that, for this particular series of plasmas, the gas dosing from the main chamber was progressively decreased from 3.0×10^{22} el/s to 1.2×10^{22} el/s keeping the auxiliary heating power, the pellet injection frequency and the pellet particle throughput unchanged at 34 MW, 35 Hz and

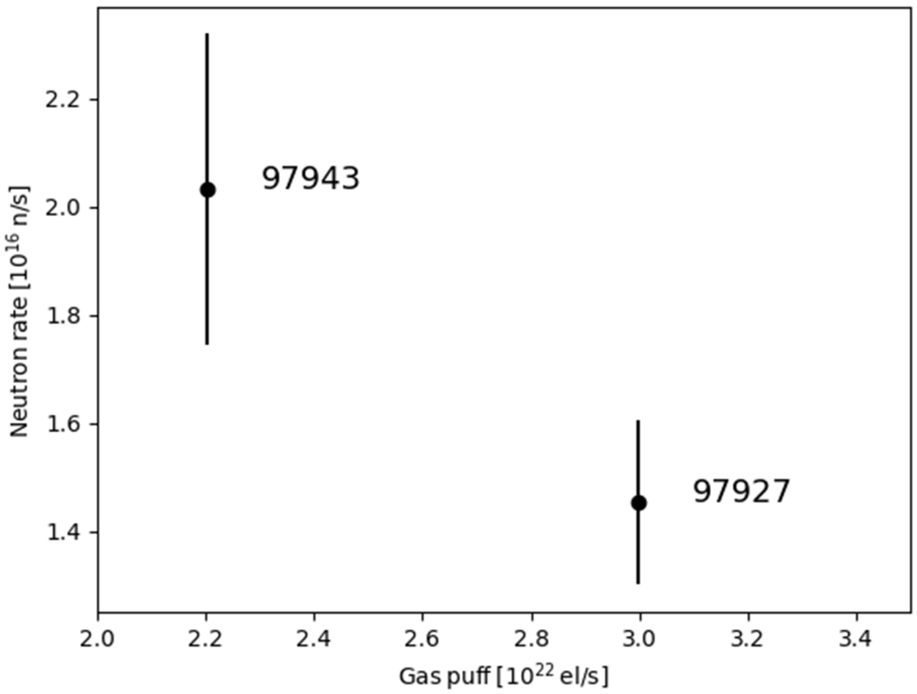

Figure 6. Neutron yield for JPN 97927 and JPN 97943 as function of gas puff, highlighting the decreasing trend of neutron rate with increasing gas throughput. The neutron yeld for JPN 97927 is averaged between 9 and 13.5 s and for JPN 97943 between 9 and 12.5 s. The error bars are the standard deviation in the intervals considered.

$\approx 1.3\times10^{22}$ el/s respectively. It should be noted that the density does not change significantly through the scan. Indeed, it is well known than on JET, in H-mode, the plasma density is not directly affected by gas puff and in some cases increasing the gas puff leads to a decrease in density due to an increased ELM frequency or a worse inter-ELM particle confinement or both. This behaviour was used as basis to develop a feed-back control of the ELM frequency using gas puff as an actuator, which was used in other scenarios with a well defined ELM frequency [12]. However, it was abandoned for the JET baseline scenario because, given the compound nature of the ELMs, the frequency was not easily measurable in real time. It can be seen from the spikes and the intensity of the BeII emission line, that, through the scan, the compound ELM activity characteristic of the JET baseline scenario at high I_p [5] weakens and stops earlier with lower fuelling, leading to less effective flushing of the W and a sharp increase of radiated power causing the disruption of the pulse. It is clear from this scan that an adequate fuelling rate is essential to sustain the ELM activity, flush the tungsten, prevent the radiate power from increasing and maintain the plasma sufficiently above L–H threshold. However, higher fuelling induces a degradation in confinement, neutron yield and fusion power, as it can be seen in figure 6, which shows the average neutron rate as function of gas puff for JET pulse number (JPN) 97927 and JPN 97943. The reason for such a reduction in performance is a complex interplay of effects including enhanced transport in the pedestal (affecting the plasma stored energy and the thermal neutron yield) and a shallower penetration of the NBI (leading to a lower beam-target neutron yield).

From a different perspective, if we consider the ratio between the power crossing the separatrix $P_{net} = P_{NBI} + P_{ICRH} - P_{rad}$ (where P_{rad} is the total radiated power from inside the separatrix) and the L–H transition power threshold (P_{L-H} as defined by Martin in [13]) we can see from figure 7 that its value decreases after the plasma transits into H-mode at $t \approx 8$ s and reaches ≈ 1 earlier for lower gas dosing. At this point the ELM activity ceases, the radiated power starts increasing steeply and the stationarity of the pulse is lost. This observation shows that both ELM pacing pellets and sufficient gas dosing are necessary to promote the ELM activity necessary for the stationary of the pulse [5] and has been exploited to design a real time control algorithm using the gas puffing rate as an actuator to keep the plasma ELM-ing and $P_{net}/P_{L-H} > 1$ [14].

The scenario optimized in D at 3.5 MA, sustained for 5 s and capable, in principle, to deliver $\leqslant 8$ MW of fusion power (depending on the available auxiliary heating power) in D–T, was subsequently realized in T and D–T in 2021, but it was not possible to sustain it for 5 s as in D [5]. The results are shown in figure 8, where we compare three JET baseline plasmas at 3.5 MA / 3.35 T in D, D–T and T respectively. In this comparison it should be noted that H pellets at 17 Hz (leading to a H concentration

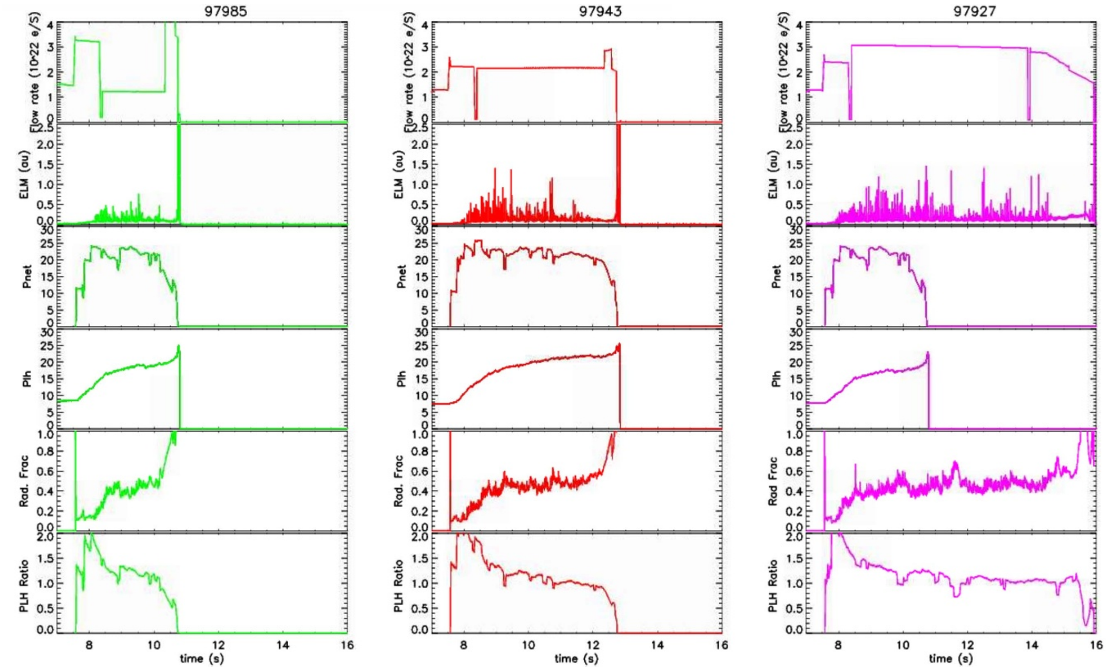

Figure 7. Gas throughput, BeII emission, P_{net}, P_{LH}, radiated power fraction and $P_{\mathrm{net}}/P_{\mathrm{L-H}}$ for three pulses from the fuelling scan shown in figure 5. $P_{\mathrm{net}}/P_{\mathrm{L-H}}$ decreases faster and faster with decreasing gas throughput leading in turn to an earlier weakening and termination of the compound ELM activity responsible for the flushing of the tungsten, an increase of the radiated power fraction an H–L back-transition and, eventually, a disruption.

of ≈20%) were injected during the main heating phase of the T plasma to promote the compound ELM activity without producing any D–T neutrons. It can be seen that while the additional heating power and the combined pellet and gas particle fuelling during the H-mode is similar for the three pulses, the average plasma electron density is higher, the radiated power is increasing faster, and the ELM activity is ceasing earlier in T than in D–T than in D.

It should be noted that the three pulses in figure 8 are not identical insofar they do not have exactly the same gas and pellet fuelling scheme. In particular the T pulse has a gas fuelling rate higher than the D and the D–T pulses. To discuss this point, it should be noted that only six pulses in T at 3.5 MA were performed on JET with metal wall, they were run before the D–T campaigns to investigate the H-mode entry phase in T and ‘bracket’ (between D and T) the expected plasma behaviour in D–T, rather than get a perfect match with D–T plasmas. A fuelling scan performed in T showed that the fuelling rate (H pellet plus T gas) of JPN 99282 was the minimum required for a T pulse to be sustained for a few seconds without going ELM-free and disrupting immediately after the L–H transition. For a pulse in T to be sustained for longer an even higher fuelling rate would have been necessary. Therefore, a perfect match at the same level of fuelling as the D and D–T pulses (JPN 96893 and JPN 99948) is not possible. However, comparison with a D pulse with fuelling rate more similar to 99282 is possible and shown in figure 9, where we compare JPN 99282 (in T) with JPN 97858 (the D pulse at 3.5 MA with the highest fuelling rate, without pellets). It can be seen that, despite the very similar fuelling rates the density is still lower in D than in T indicating the existence of an isotope effect. In fact, an isotope effect on JET, affecting especially the particle transport channel, has been documented and analysed via gyrokinetic simulations (see, for example [15]).

Figure 10 shows that the electron density at $t = 6.86$ s, just before the L–H transition, is almost identical for the three pulses, whereas the on-axis electron temperature in the T pulse is 3 keV as opposed to 2 keV in the D and D–T pulse. On the other hand, figure 11 indicates that at $t = 8.86$ s, 1 s after the start of the NBI heating and the L-H transition and before the T and the D–T pulses are stopped by the tokamak protection system reacting to the excessive radiated power, the electron density profiles are significantly different, exhibiting a higher electron density at the top of the pedestal in T than in D–T than in D. The electron temperature profiles are relatively similar in D–T and T and 10%–20% lower in D, whereas the ion temperature profiles are relatively similar in D and T and 25% higher in D–T.

In the transition from D, to D–T and to T we observe a similar trend in the ratio $P_{\mathrm{net}}/P_{\mathrm{L-H}}$ to the one observed in the gas scan in D at 3.8 MA. In particular, as shown in figure 12 we see that the higher density in T than in D–T than in D results in a faster decrease of the $P_{\mathrm{net}}/P_{\mathrm{L-H}}$ ratio (likely due

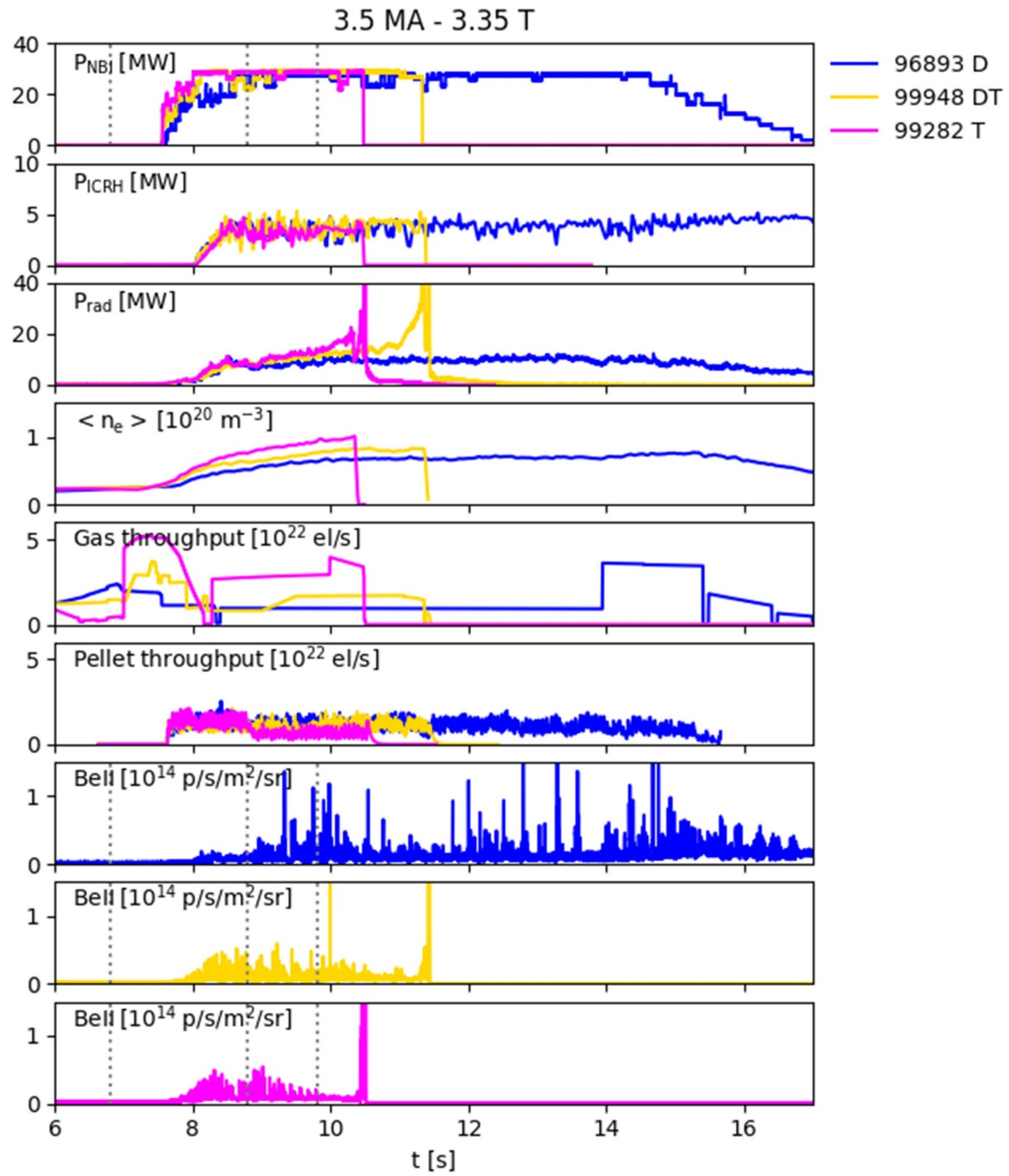

Figure 8. Time traces of the main plasma parameters of three 3.5 MA / 3,35 T JET pulses in D, D–T and T with similar heating power and gas and pellet fuelling. H pellets at 17 Hz were injected in the T plasma to promote the compound ELM activity without producing any D–T neutrons. The compound ELM activity stops earlier and earlier with increasing effective isotope mass and only the D pulse can be sustained for 5 s. The first two vertical lines indicate the times of the profiles in figures 10 and 11 respectively, whereas the third vertical line indicates the time when the T pulse is stopped by the plasma protection system for excessive radiated fraction.

to higher radiated power) and a progressively earlier loss of compound ELM activity in D–T and in T, compromising the stationarity of the pulse. Note that to take into account the dependence on the isotope mass of the L–H threshold proposed in [16] the estimate of $P_{\mathrm{L-H}}$ obtained from the Martin scaling has been multiplied by 0.8 (2/2.5) and 0.67 (2/3) for the D–T and the T plasma respectively. Moreover, it should also be noted that, for the T pulses, the H concentration due to the pellet injection was not taken into account in the estimate of $P_{\mathrm{L-H}}$.

Despite the fact that the D–T pulse could not be sustained for 5 s, the peak fusion power achieved in the JET baseline scenario at 3.5 MA was 8.3 MW, in line or even exceeding the value extrapolated from the performance of D plasmas assuming the same density at the top of the pedestal and a 50–50 D–T plasma isotope mix [5]. However, the extrapolations assumptions failed to predict and to take into account the different pedestal density and ELM behaviour in going from D to D–T. This highlights the

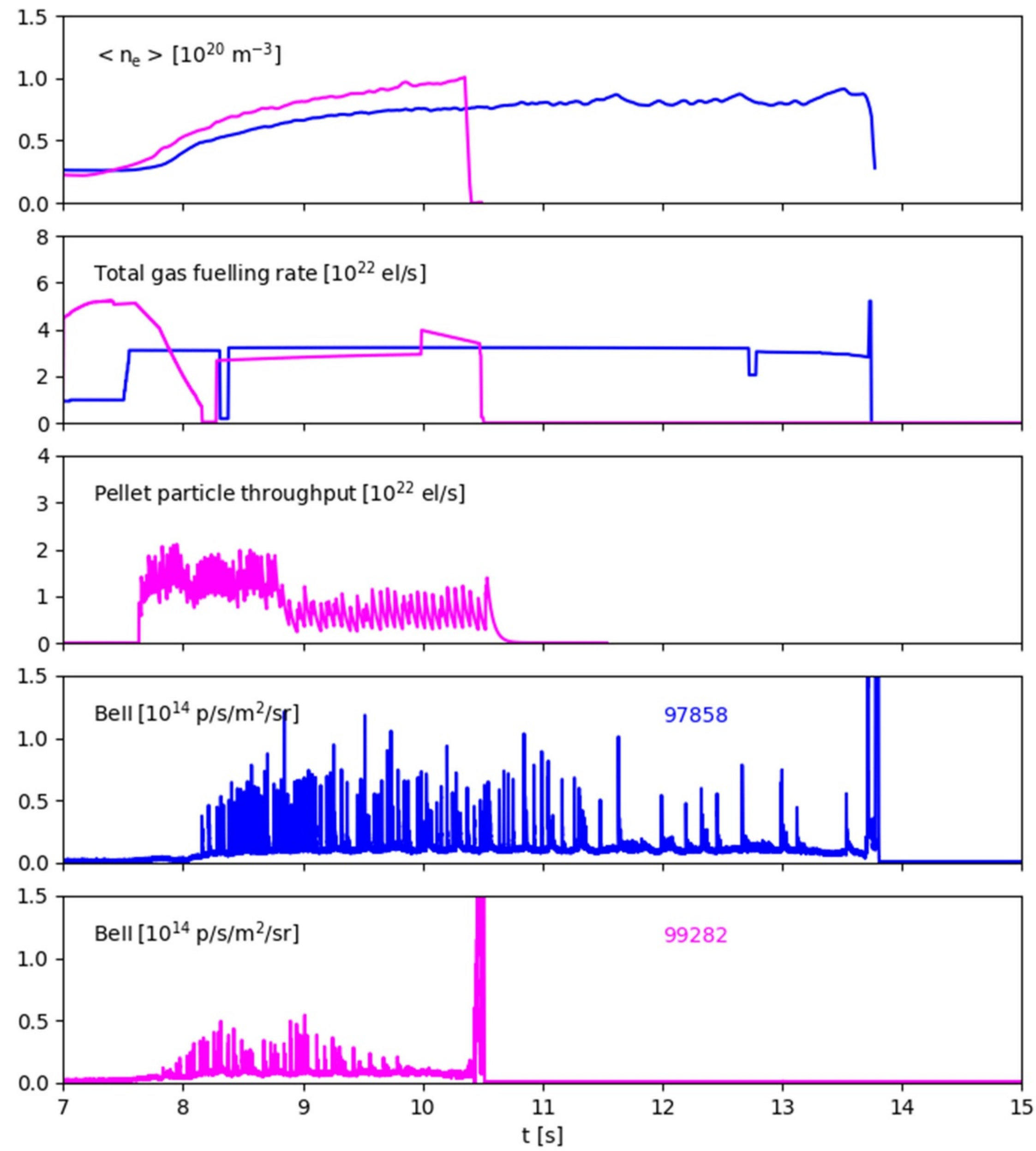

Figure 9. Time traces of the density, gas and pellet fuelling, and BeII emission (representing ELM activity) of two 3.5 MA / 3.35 T JET pulses in D (JPN 97858) and T (JPN 99282) with similar total gas fuelling. H pellets at 17 Hz were injected in the T plasma to promote the compound ELM activity without producing any D–T neutrons, whereas the D plasma has no pellets.

need for a predictive model for the transport in the pedestal including isotope effects. Such a model is not available yet but several approaches are being pursued [17].

In order to understand which isotope effect might be responsible for the different behaviour of the plasmas in D and D–T, we performed three kinds of analysis.

Firstly, we looked at the kinetic profiles in the pedestal for JPN 96893 (in D) and 99948 (in D–T). It is worth noting that in the compound ELM regime characteristic of the JET baseline plasma at $I_p \geqslant 3.0$ MA, large type-I ELMs are followed by trains of smaller ones. As mentioned earlier, the ELM induced transport regulates the density at the top of the pedestal and flushes the W from the plasma [10]. The kinetic profiles preceding a large ELM are shown in figure 13, from which it can be seen that the pre-large ELM $n_{e,ped}$ is larger in D–T than in T whereas $T_{e,ped}$ is similar. There seems to be therefore a clear isotope effect affecting the particle confinement in the pedestal. Such an effect has been observed in other JET scenarios [18].

Secondly, we performed an ideal MHD stability analysis for the same couple of pulses based on the kinetic profiles shown in figure 13. The workflow used in the analysis incorporates HELENA (for the equilibrium reconstruction) and MISHKA (for the stability analysis) and is described in [19]. The results

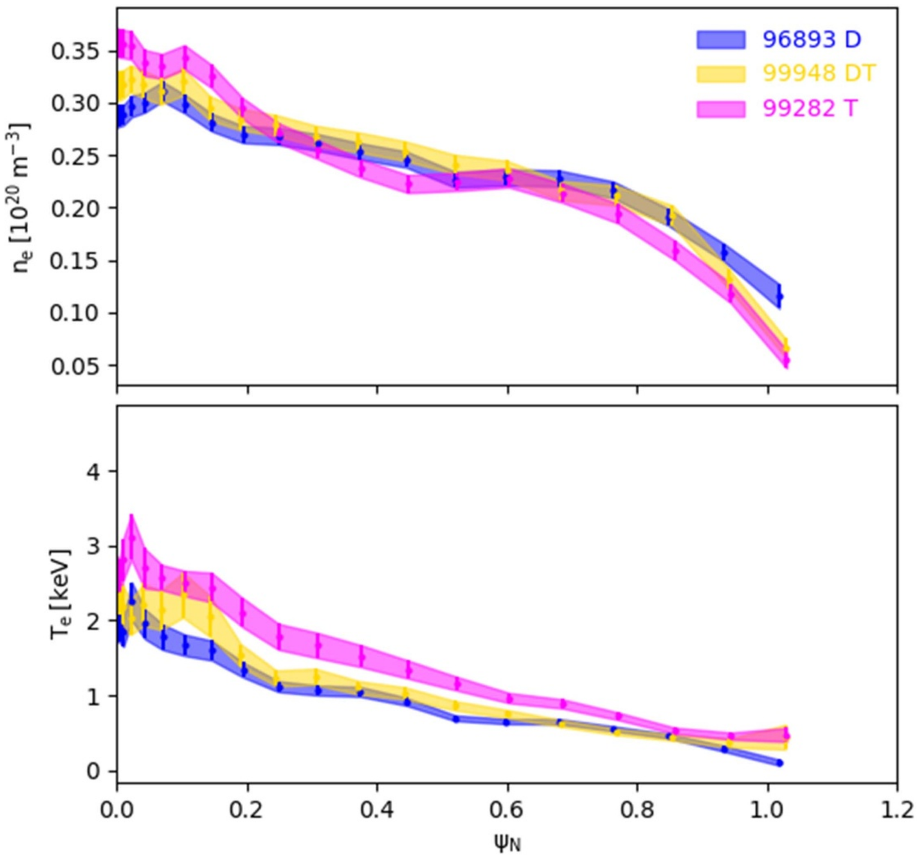

Figure 10. Electron density and temperature profiles for the three pulses shown in figure 8 at $t = 6.86$ s (1 s before the start of the NBI heating and the L–H transition). The ion temperature profile is not shown as it was not measured at this time.

are shown in figures 14 and 15 and indicate that there is no clear difference between the two pulses. In particular, neither the D nor the D–T plasma is in the peeling-ballooning unstable region, but pushing towards the ballooning boundary. There is a qualitative difference between pre-large ELMs and pre-small ELMs profiles, insofar large-ELM equilibria are closer to the stability boundary than the small-ELM cases. Moreover, the stability boundaries are in the same region of the $\alpha_{\max} - j_{\max}/\langle j \rangle$ diagram both for D and D–T plasmas. Therefore, no clear isotopic effect on the pedestal ideal MHD stability is observed in this regime. This could be expected and was documented for a different JET scenario in [20]. Resistive MHD stability analysis is planned but it is beyond the scope of this paper and could give a different answer depending on the quantitative effect of non-ideal effects in scenarios featuring relatively high pedestal temperature ($T_{e,ped}$, $T_{i,ped} \approx 1$ keV), low separatrix density and therefore low pedestal collisonality [21].

Thirdly, we analysed the behaviour of the W density, estimated as the quasi-continuum emission intensity divided by line-average density in the three pulses presented in figure 8. The results are shown in figure 16, from which it can be seen that there is no clear isotope effect affecting the W density in D, D–T and T both before and immediately after the L–H transition. Indeed, a divergence from stationarity and an increase in W density seems to be a consequence of the weakening of the compound ELM activity and the W flushing. Therefore, a plausible interpretation of the chain of events leading to a disruption in D–T and T (but not in D) is the following: the W present in the plasma at the start of the pulse does not depend on the isotope mix, the different evolution of the main gas density leads to a faster increase of the radiation in T than in D–T than in D, this in turn causes the compound ELM activity to stop earlier with the heavier isotope species, when the compound ELM activity is weakened the W is not efficiently flushed anymore, the radiated power increases sharply causing a H–L back transition and, eventually, a disruption.

Finally, as we did for the D plasmas [22], we run fully predictive *a posteriori* transport simulations of JPN 99948 with the JINTRAC suite of codes [23] equipped with the QuaLiKiZ transport model [24] to test whether we could reproduce the experimental results in D–T. In the simulations presented in this paper we solve for D (and T, when present) density, Be, Ni and W density, electron and ion temperature and impose the toroidal rotation from measurements. The particle, impurity and heat anomalous

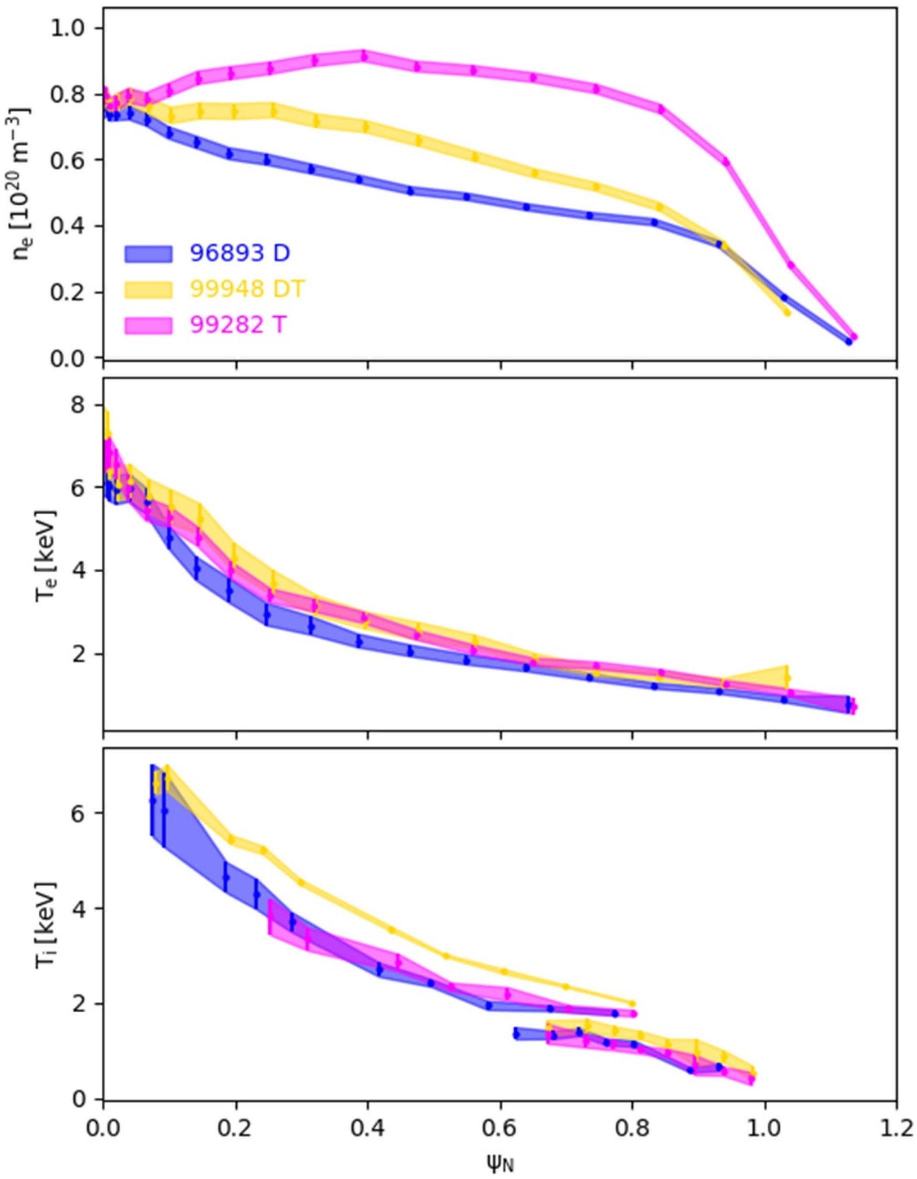

Figure 11. Electron density and electron and ion temperature profiles for the three pulses shown in figure 8 at $t = 8.86$ s (1 s after the start of the NBI heating and the L–H transition).

transport in the core is provided by QuaLiKiZ, whereas the neoclassical transport is given by NCLASS [25]. In the edge transport barrier (ETB), the width of which is fixed from the experimental profiles, we prescribe ion end electron heat conductivities $\chi_i = \chi_e$ in order to match the experimental ion and temperature profile, we assume a heat conductivity over particle diffusivity ratio $\chi/D = 4$ and we adjust the intensity of the gas fuelling in a feed-back loop to follow the value of the density at the top of the ETB. Gas puffing and wall recycling particle sources are calculated by FRANTIC [26] and pellet particle sources are approximated with a ionization source with Gaussian shape centred at $\rho = 0.9$ and of width 0.15. The NBI particle and heat deposition is calculated by PENCIL [27] and the ICRH heat deposition with PION [28], all of them self-consistently with the evolution of the profiles. The synergy between NBI and ICRH is taken into account in the modelling. The initial and boundary conditions are taken from the experiment. n_e and T_e come from Thomson scattering measurements and the impurity mix is obtained from a multi-diagnostic analysis described in [29] and the total content of each impurity was kept constant during the simulation. Initial D and T densities are derived from quasi-neutrality. The equilibrium is self-consistently calculated by the equilibrium solver ESCO [30]. Differently from what we did before DTE2, when we assumed the same initial density profiles and the same value of the density at the top of the pedestal to extrapolate the results obtained in D to D–T, in this case we still predicted the evolution of the D, T, Be, Ni and W density, and of the electron and ion temperature, but imposed, the initial and top of the pedestal condition from the experiment (the plasma rotation was also

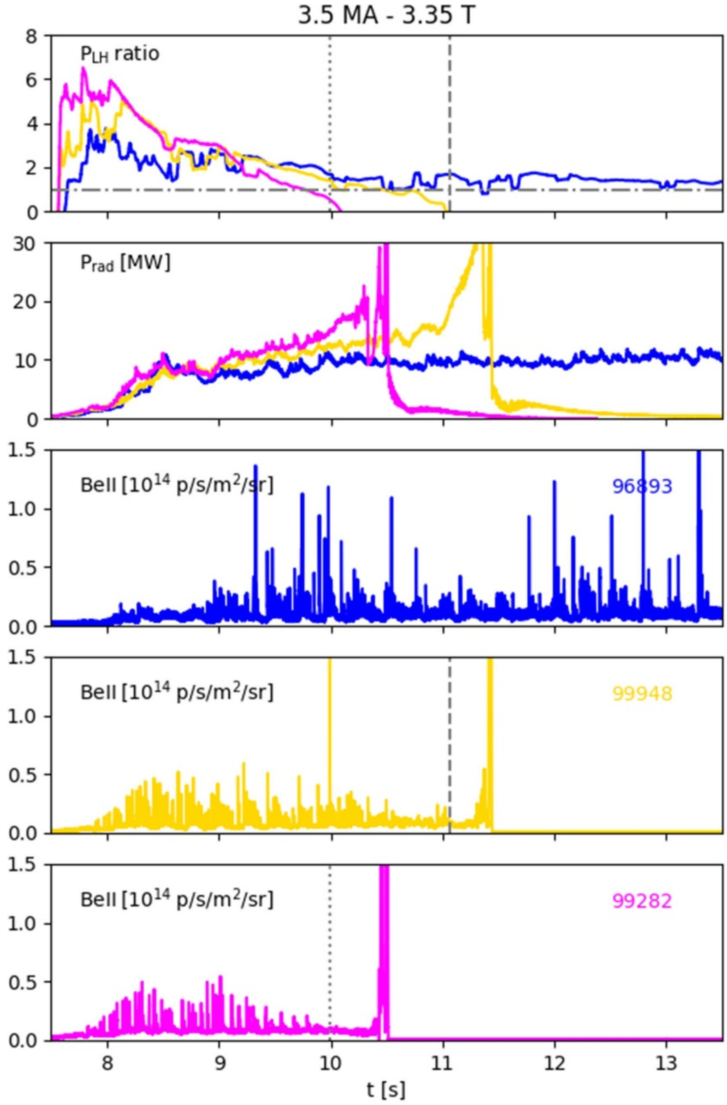

Figure 12. $P_{\rm net}/P_{\rm L-H}$, P_{rad} and BeII emission for the three pulses shown in figure 8. $P_{\rm net}/P_{\rm L-H}$ decreases faster and faster with increasing effective isotope mass and only the D pulse can be sustained for 5 s. The two vertical lines indicate the times when the D–T and the T pulse are stopped by the plasma protection system for excessive radiated fraction.

imposed from experimental measurements). The results are shown in figure 17, from which it can be seen that, when the experimental initial condition and evolution of the density at the top of the pedestal are imposed the QuaLiKiZ transport model captures the observed increase in $\langle n_{\rm e}\rangle$ and in $P_{\rm rad}$ for a constant W particle content. This result highlights the importance of a predictive model for the pedestal behaviour (including realistic particle source) in order to be able to predict the behaviour of the core plasma. It should be noted that such a model should predict not only the behaviour of the pedestal in stationary conditions, but also its evolution, including the weakening of the compound ELM activity responsible for the loss of stationarity and the ultimate radiative collapse when $P_{\rm net}/P_{\rm L-H}$ becomes lower than a certain value, as observed in the experiment.

4. JET baseline scenario at 3.0 MA and recovery of a stationary pulse

The analysis of the experimental results obtained on JET at 3.5 MA in D–T showed that sustained ($\geqslant$5 s), high-current ($I_{\rm p}\geqslant 3.5$ MA) and record performance ($P_{\rm fus}\geqslant 10$ MW) were incompatible with a W divertor for the auxiliary heating power available for the JET baseline scenario in DTE2. Moreover, they indicate that the fuelling scheme developed in D to optimize the fusion power was not directly transferable to D–T operations.

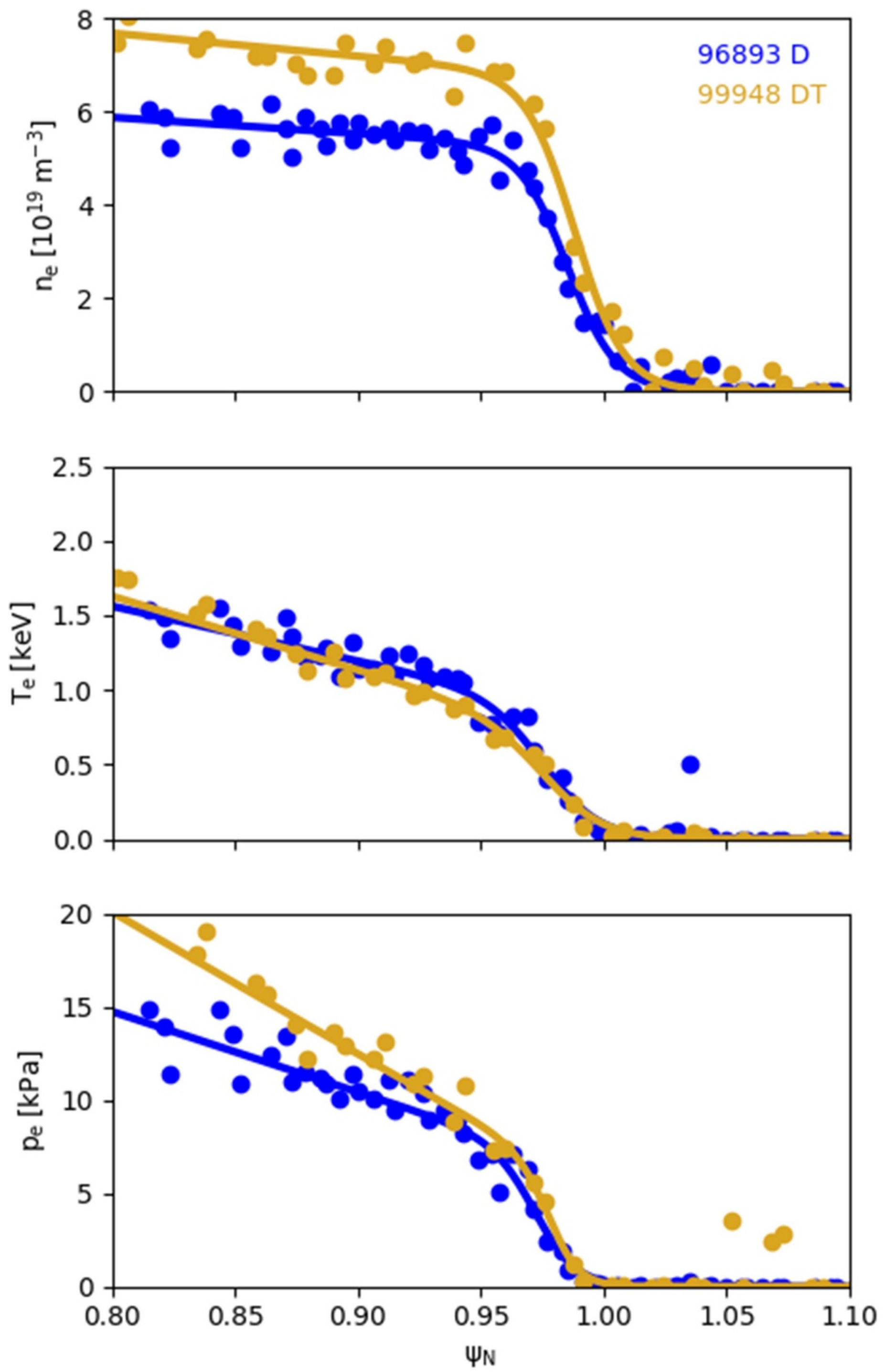

Figure 13. Electron density, temperature and pressure in the edge transport barrier (ETB) for JPN 96893 (D) and JPN 99948 (D)–(T). For JPN 96893 data are taken 10 ms to 1 ms before large ELMs between 11 and 13 s, for JPN 99948 data are taken 10 ms to 1 ms before large ELMs between 9.8 and 10.4 s.

In order to achieve a scenario that could be sustained for more than 5 s in D–T two options are available: reduce the plasma current to reduce the density and increase the fuelling rate to maintain the compound ELM activity, accepting at the same time a non-optimal plasma performance. Both of the above options were implemented in the DTE3 campaign in 2023, where D–T JET baseline plasmas were run at 3.0 MA / 2.85 T with increased gas fuelling.

It is worth mentioning that the DTE3 campaign on JET was different from DTE2 from several points of view. In particular, more heating power ($P_{aux}\leqslant 35$ MW) was available, thanks to an extra neutral beam injector (PINI) not available in DTE2, and the NBI system was operated in full D (as opposed to 50–50 D–T as in DTE2). Moreover, the campaign priorities were different and did not focus on high-current and high-performance plasmas. Consequently, no time was allocated to the optimization of the

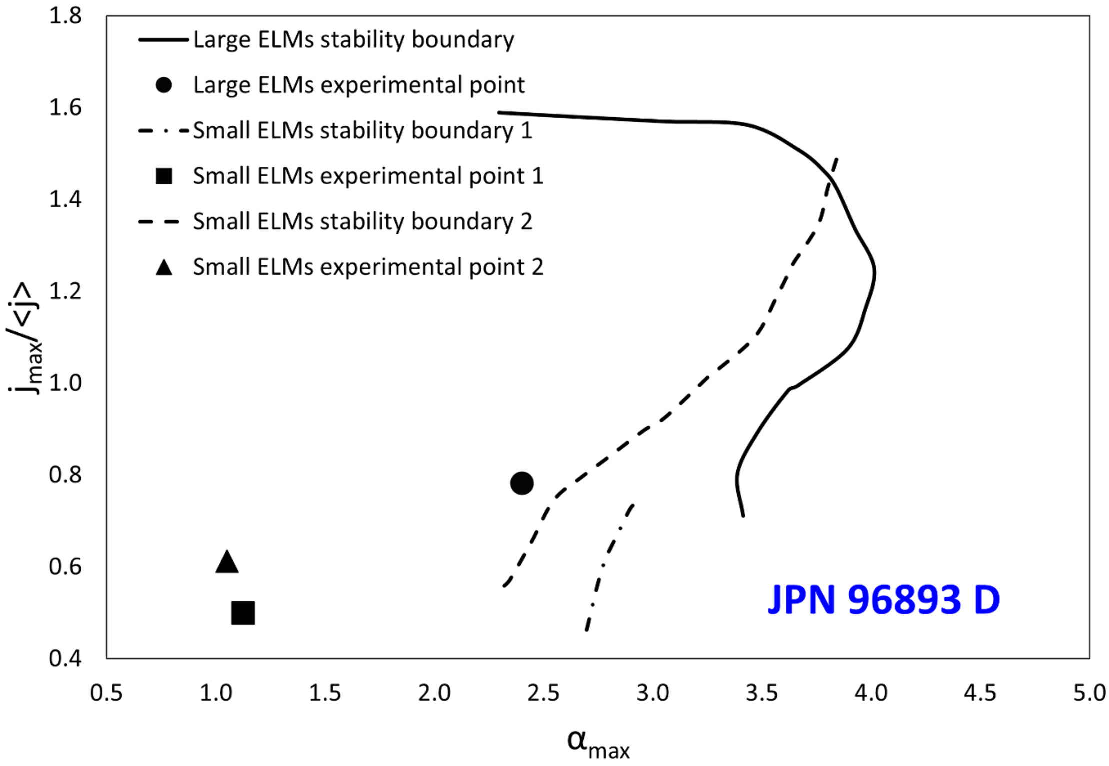

Figure 14. Ideal MHD stability diagram for JPN 96893. The input profiles are taken between 11 and 13 s. Large ELMs 1: 10–1 ms before large ELMs; small ELMs 1: 1.0 ms to 0.5 ms before small ELMs; small ELMs 2: 0.6 ms to 0.1 ms before small ELMs. The distinction between large and small ELMs is somewhat arbitrary and based on the intensity of the BeII emission light during an ELM.

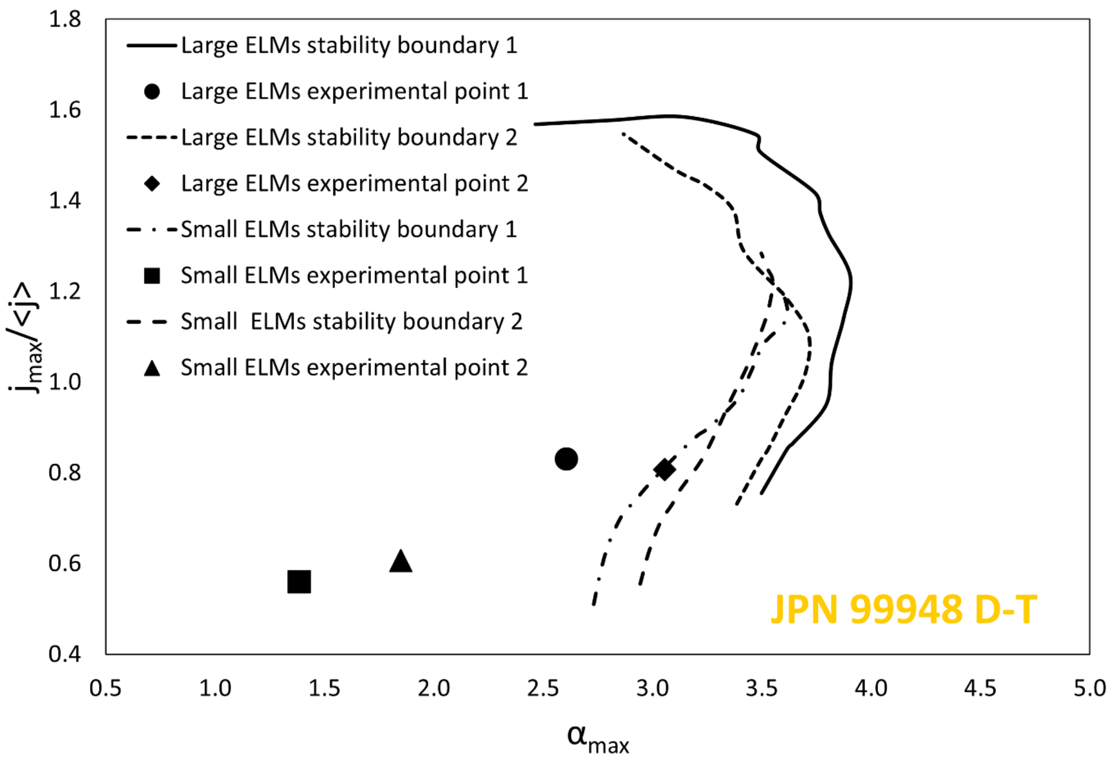

Figure 15. Ideal MHD stability diagram for JPN 99948. The input profiles for the cases labelled 1 are taken between 8.6 and 9.1 s. Large ELMs 1: 10 to 0.5 ms before large ELMs; small ELMs 1: 1.0 ms to 0.5 ms before small ELMs. The input profiles for the cases labelled 1 are taken between 9.8 and 10.4 s. Large ELMs 2: 10 ms to 0.5 ms before large ELMs; small ELMs 2: 1.0 ms to 0.5 ms before small ELMs.

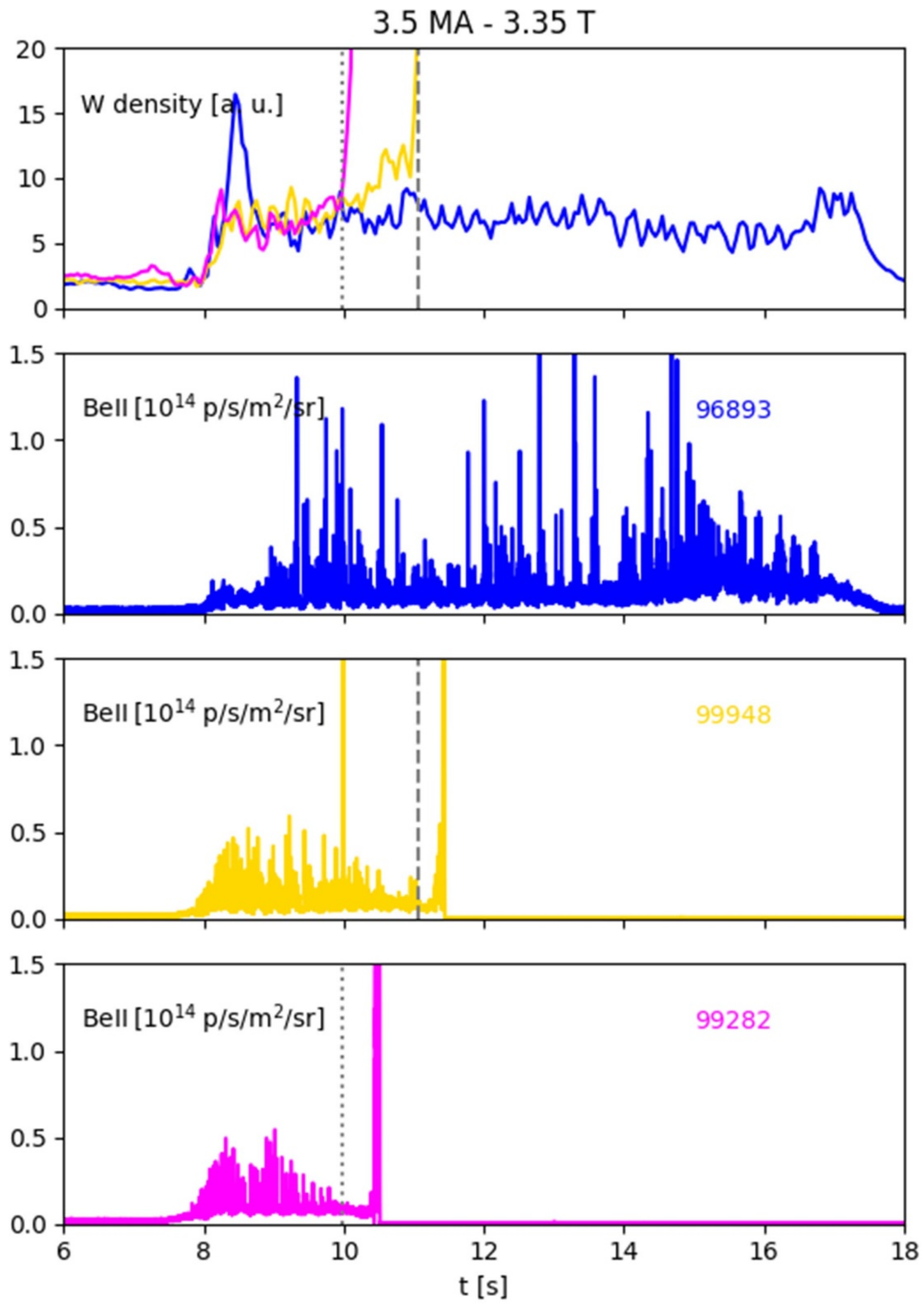

Figure 16. Tungsten density (quasi-continuum emission divided by line-integrated electron density) and BeII emission (representing ELM activity) for the three pulses shown in figure 8. The two vertical lines indicate the times when the D–T and the T pulse are stopped by the plasma protection system for excessive radiated fraction.

JET baseline high-current scenario, which was deemed too risky for the integrity of the machines for the reasons explained in section 2 [4].

In total, the path to developing a 5 s JET baseline scenario at 3.0 MA in D–T consisted of three technically successful pulses (JPN 104661, JPN 104662 and JPN 104663) shown in figures 18–20. In the first attempt (JPN 104661) we deployed all the available auxiliary heating power, kept the D pellet injection frequency unchanged at 35 Hz and required a T gas throughput of 0.8×10^{22} el/s. As can be seen from figure 18, the fuelling recipe, chosen to guarantee at the same time an acceptable reduction of the performance and a balanced source of D and T atoms, proved insufficient to maintain the compound ELM activity for the entire programmed duration of the pulse, which was stopped by the machine protection system because of the excessive radiated power fraction, just before $t = 12$ s. In the second attempt (JPN 104662), to further promote the compound ELM activity and make the pulse stationary, we increased the T gas puff by 0.3×10^{22} el/s and added an additional D gas puff of 0.37×10^{22} el/s. Figure 19 shows that this successfully prevented the weakening of the compound ELM activity, but the pulse was stopped

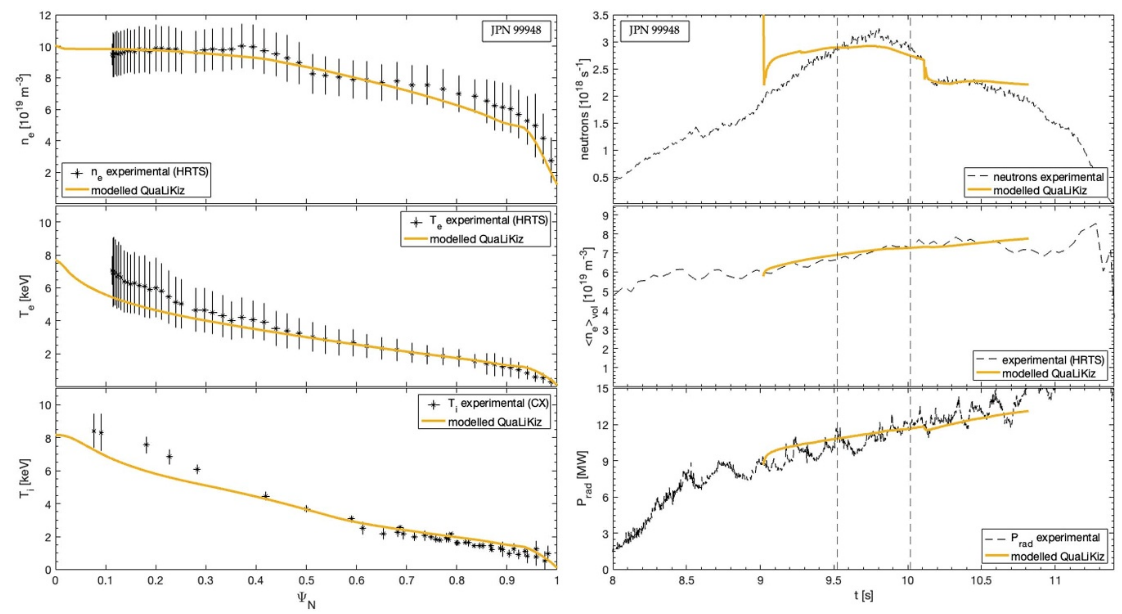

Figure 17. JINTRAC predictive modelling results for JPN 99948 with the QuaLiKiZ transport model. Left from top to bottom: electron density, electron and ion temperature. Right from top to bottom: neutron yield, volume-averaged density and radiated power. Initial condition and density at the top of the pedestal are imposed from experiment and not assumed on the basis of D plasma. The increase in density and radiated power is captured by the simulation.

again by the protection system because of the onset of a $n = 2$ neo-classical tearing mode (NTM) at $t \approx 11.5$ s. In the third attempt (JPN 104663), to avoid the onset of an NTM, we reduced the NBI heating power by ≈ 2 MW and successfully reached the programmed end of the pulse (figure 20), which disrupted only in the current ramp-down due to a non-optimized termination scheme.

Figure 21 [4] shows that, in terms of fusion performance, the 5 s, 3.0 MA JET baseline scenario (non-optimized, as no experimental time was dedicated either to perform a finer fuelling scan to optimize the performance or to replicate the scenario at 3.5 MA, where we could have applied all the available NBI heating power) produced 18 MJ of fusion energy, much less than the record 42 MJ and 69 MJ of fusion energy achieved in the hybrid and the T-rich scenarios respectively, both of which operated at 2.3 MA and in type-I ELM regime [6, 31]. However, it is not far below the 27 MJ of fusion energy obtained in the JET ITER baseline scenario at 3.0 MA (highly optimized), with 35 MW of auxiliary heating power, Ne seeding, high triangularity plasma shape and extended for a longer time window.

Figure 22 shows that also in this case fully a predictive simulation with JINTRAC-QuaLiKiZ of the 3.0 MA sustained pulse captures the main experimental parameters. Moreover, integrated transport modelling indicates that pure D NBI leads to a higher concentration of D in the plasma core than in DTE2. This is shown in figure 23 where we plot the predicted T concentration for pulses at 3.0 and 3.5 MA in DTE2 (where 50–50 D–T NBI were used) and for a pulse at 3.0 MA in DTE3 with pure D NBI.

This prediction is reinforced by the TRANSP analysis [32, 33] illustrated in figure 24. The results show that assuming a 50–50 D–T mixture in the plasma core and a 2.5% Be concentration leads to a $\approx$60% overestimate of the experimental neutron yield. Imposing the D–T concentration predicted by JINTRAC-QuaLiKiZ reduces the overestimate to $\approx$52%, but it is not sufficient to recover the experimental results. In addition, assuming a higher concentration of Be (5.8%, compatible with $Z_{\text{eff}} = 1.8$, which is 20% higher than the experimental measurement from Bremsstrahlung) further reduces the discrepancy to $\approx$18%, but not completely. Finally, introducing an anomalous diffusivity for the beam fast ions of 2 $\text{m}^2\,\text{s}^{-1}$, further reduces the overestimate to $\approx$3%. The analysis shows that the enhanced dilution due to the higher Be concentration is responsible for the greatest improvement in the agreement with the experimental neutron rate (34%), whereas the fast ion anomalous diffusivity contributes for 15% and a non perfectly balanced 50–50 D–T mix for 8%.

As for the causes of the fast ion anomalous diffusion, we note that the main core MHD activity observed in the JET baseline scenario are sawteeth, NTMs and fishbones. Although a detailed study of the influence of these phenomena on the neutron rate has not been completed yet, clear correlations have been observed between sawteeth, fishbones and losses of fast-ions and fusion-born alpha-particles detected with FILD. In particular, in JPN 104663, the neutron rate degradation is attributed to redistribution of the beam fast-ions due to sawteeth and subsequent reduction of the beam-target fusion yield.

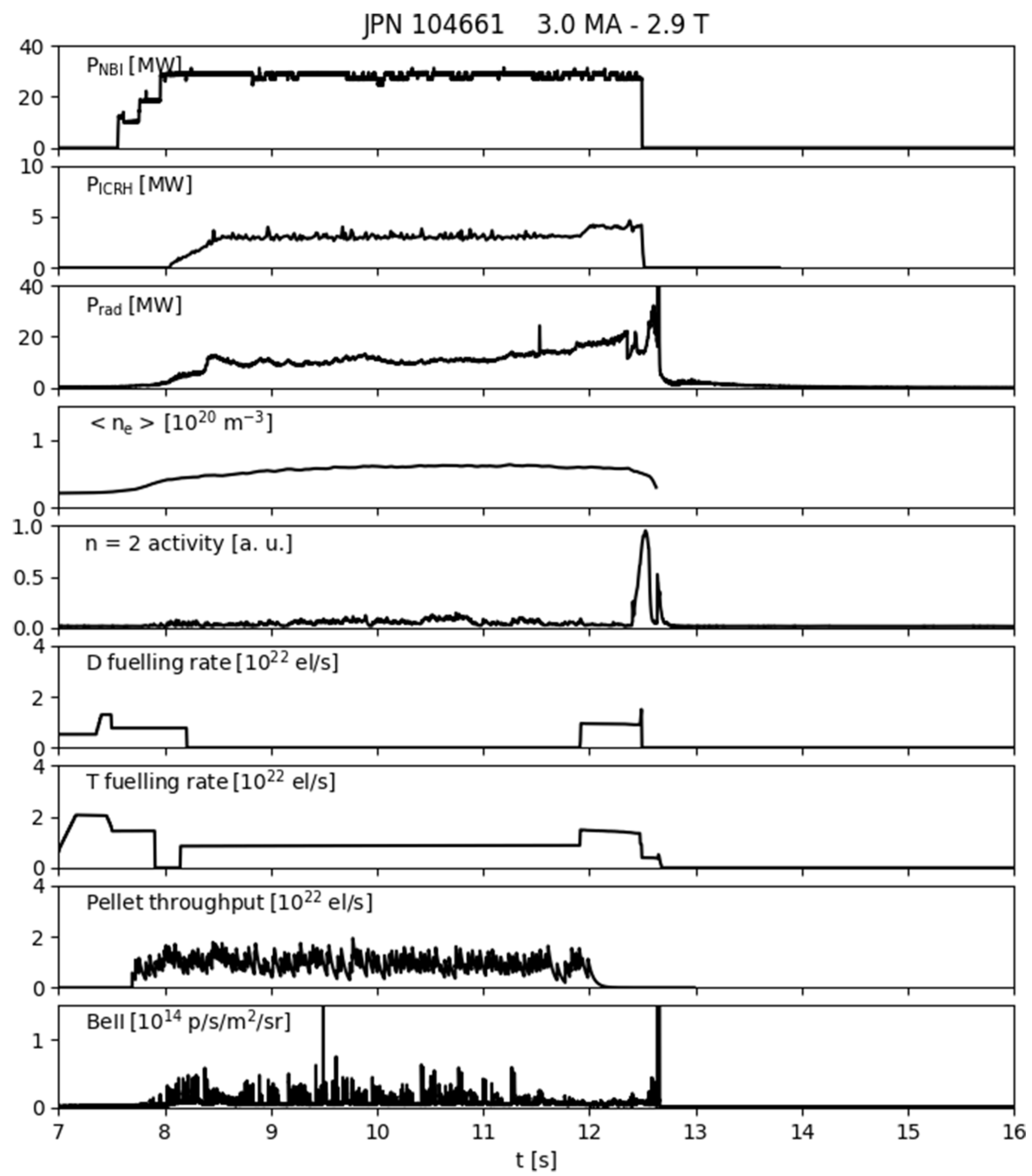

Figure 18. Time traces for JPN 104661 in D–T at 3.0 MA / 2.8 T performed in DTE3. The fuelling rate is insufficient to make the shot stationary.

TRANSP analysis indicates also that, in these pulses the percentage of thermal and beam-target neutrons is approximately 33% and 67%, respectively.

5. Discussion and conclusions

In the previous sections we have shown that a high-current ($I_p = 3.5$ MA), high fusion performance ($P_{fus} \approx 10$ MW) scenario in D–T could not be sustained on JET with auxiliary power $\leqslant$32 MW for 5 s and that, in order to sustain the baseline scenario, it was necessary to reduce the plasma current to 3.0 MA and increase the fuelling rate with a significant reduction in fusion performance.

However, it is legitimate to ask what would the result have been had we run a 3.5 MA plasma in D–T with all the heating power available in DTE3 ($P_{aux} \approx 35$ MW). In order to answer this question, a step-up in plasma current and some fuelling optimization would have been required, but was not performed because it was decided to dedicate the available machine time to other experiments.

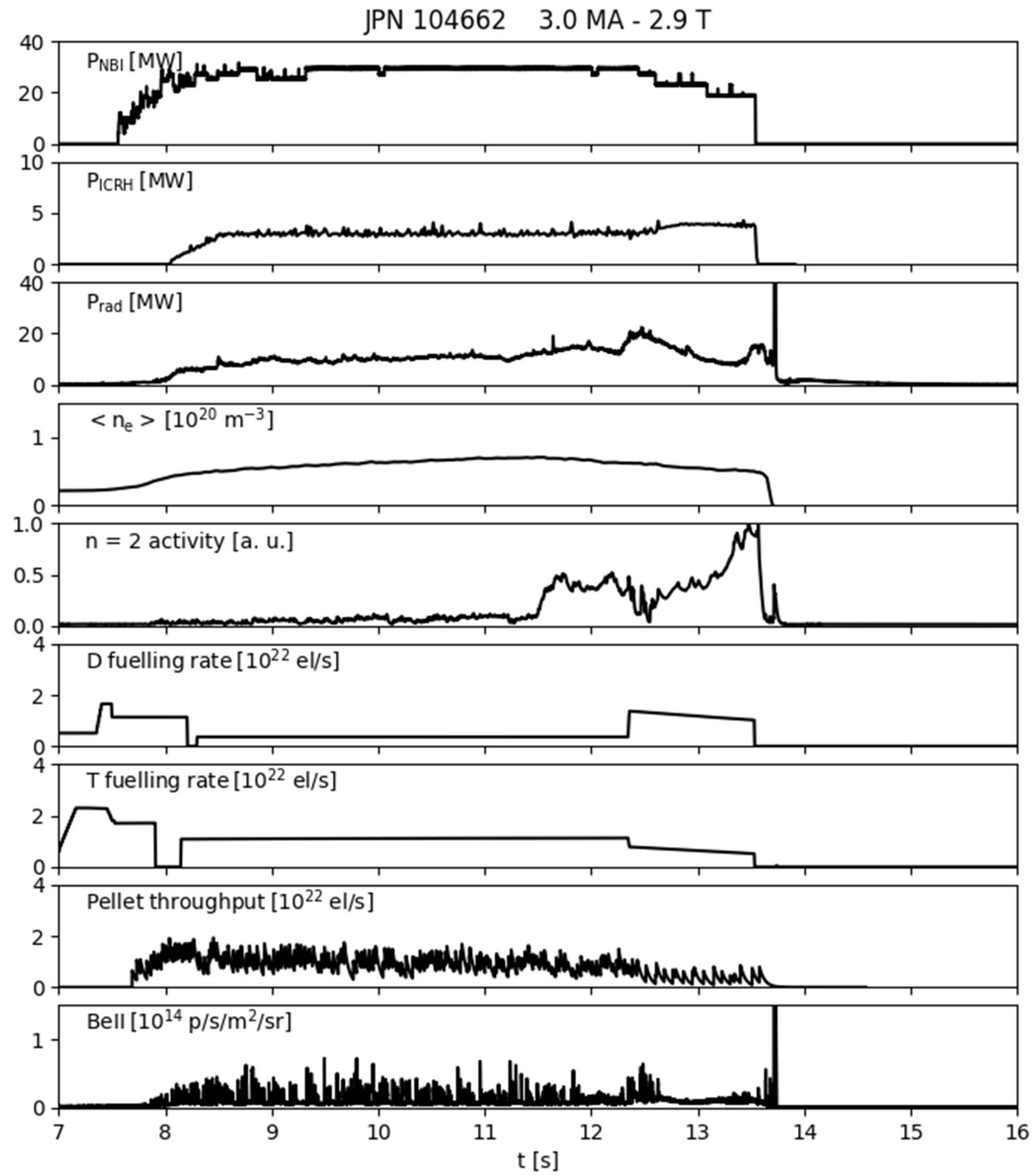

Figure 19. Time traces for JPN 104662 in D–T at 3.0 MA / 2.8 T performed in DTE3. Although in this case the fuelling would have been sufficient to maintain the compound ELM activity and make the shot stationary an $n = 2$ NTM is triggered at ≈ 11.5 s and causes the pulse to be terminated before the pre-programmed end time.

Nevertheless, it is natural to imagine two possible outcomes: a) the extra power with respect to DTE2 could have been sufficient to sustain the plasma for 5 s and achieve sustained fusion power close or higher than in pulse 99948; or b) the required level of fuelling to sustain the pulse for 5 s could have been still too high and record performance would have remained unachievable despite the higher heating power available. Unfortunately, predictions of the outcome based on modelling are difficult because we cannot accurately predict the density and compound ELM behaviour in response to fuelling and heating power.

Despite the fact that the answer to the question of how much heating power would have been necessary to achieve a sustained record-performance plasma on JET with $I_p \geqslant 3.5$ MA remains open, several lessons were learnt by developing over several years a high-current scenario in D, D–T and T with a Be/W wall. First of all, it is clear that high fusion performance and high-current operation on JET with a W divertor required all systems performing at maximum design specifications with high reliability. Secondly, it appears that the main development of a scenario meant for operation in D–T should be carried out in D–T. In fact, porting a scenario optimized for fusion performance in D to D–T is not

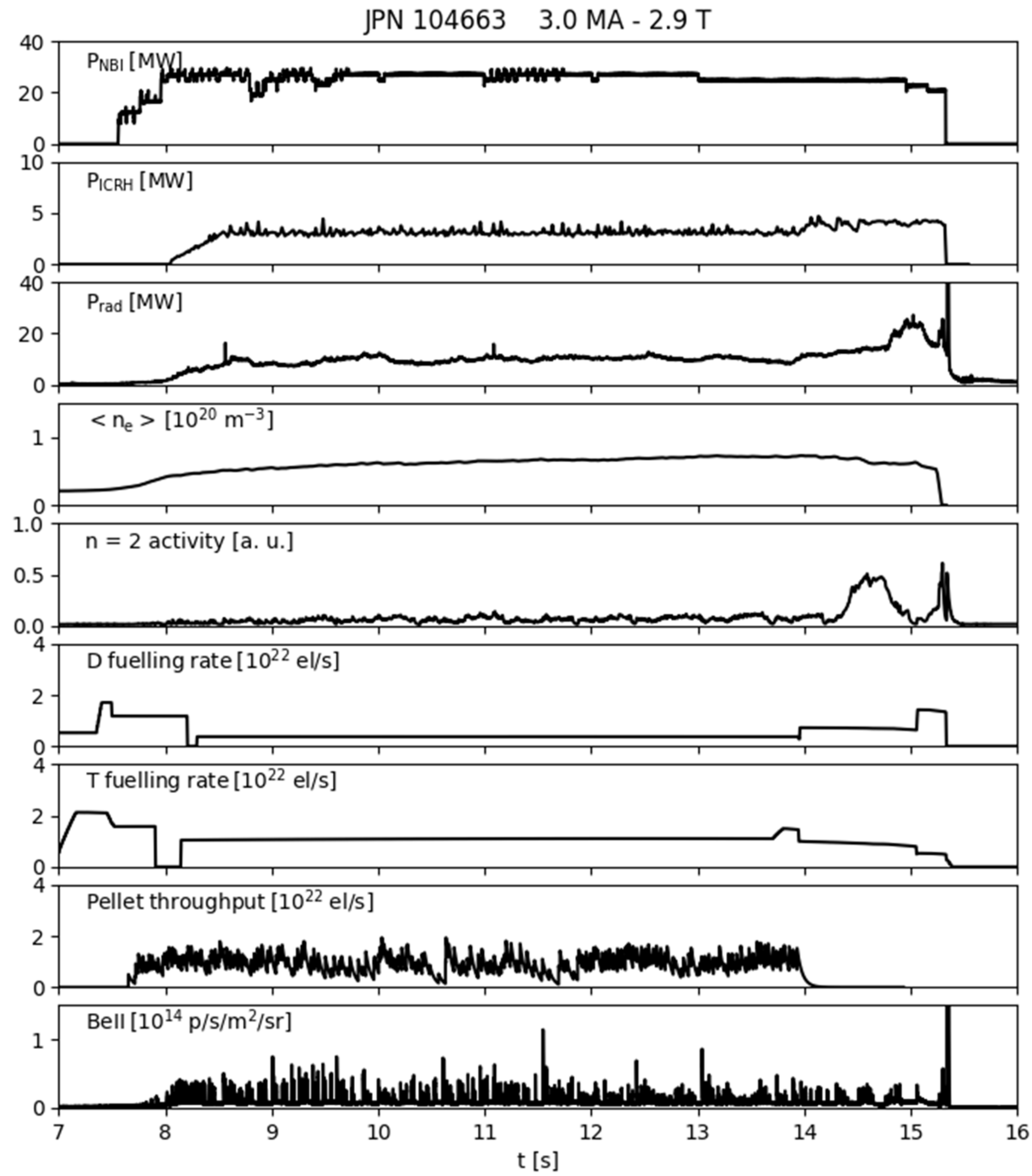

Figure 20. Time traces for JPN 104662 in D–T at 3.0 MA / 2.8 T performed in DTE3. Reducing the heating power by ≈ 2 MW eliminates the NTM and allows the pulse to be extended until the pre-programmed end time.

straightforward due to different plasma confinement properties (especially in relation to particle transport). In addition, extrapolation from D to D–T is also not straightforward due to the lack of predictive models for the plasma pedestal including isotope effects and for the ELM behaviour. It should be also noted that operations in T were not particularly useful to mitigate the risks of high-current operation in D–T. Finally, we confirmed that it is necessary to have a mechanism to control the main gas and tungsten density (in the case of the JET baseline scenario at high current this was provided by a compound ELM activity).

In conclusion, the development of a high-current scenario on JET for high performance D–T operation was only partially successful. A scenario at 3.5 MA capable, in principle of delivering $P_{fus} \leqslant 10$ MW in D–T was successfully developed in D and sustained for 5 s. When realized in D–T, the same scenario achieved peak $P_{fus} = 8.3$ MW (in line with predictions), but could not be sustained for 5 s due to the different behaviour of the pedestal density in D–T and the insufficient auxiliary heating power available in DTE2. The heating power requirements for a sustained record-performance D–T JET baseline plasma at $I_p \geqslant 3.5$ MA remain an open question.

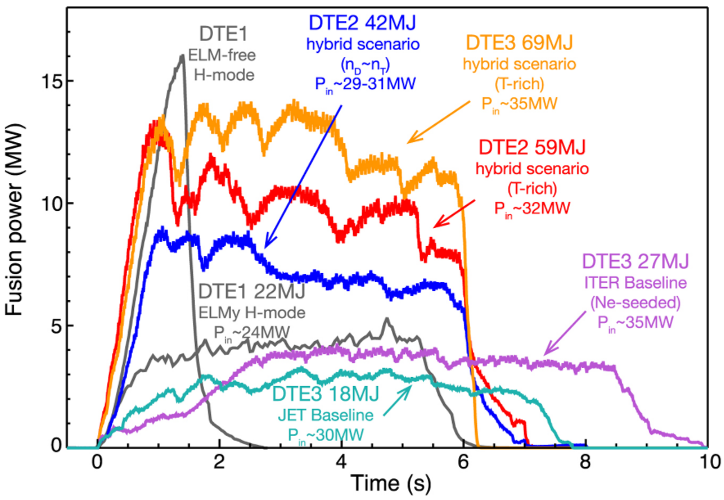

Figure 21. Fusion power obtained for different JET scenarios in DTE1 (1997), DTE2 (2021) and DTE3 (2023). The JET baseline scenario sustained for 5 s at 3.0 MA (aqua) falls ≈ 1 MW below the JET ITER baseline scenario at the same current obtained in DTE3 (purple) and the ELMy H-mode scenario obtained at 3.8 MA in DTE1 (grey). Reproduced from [4].

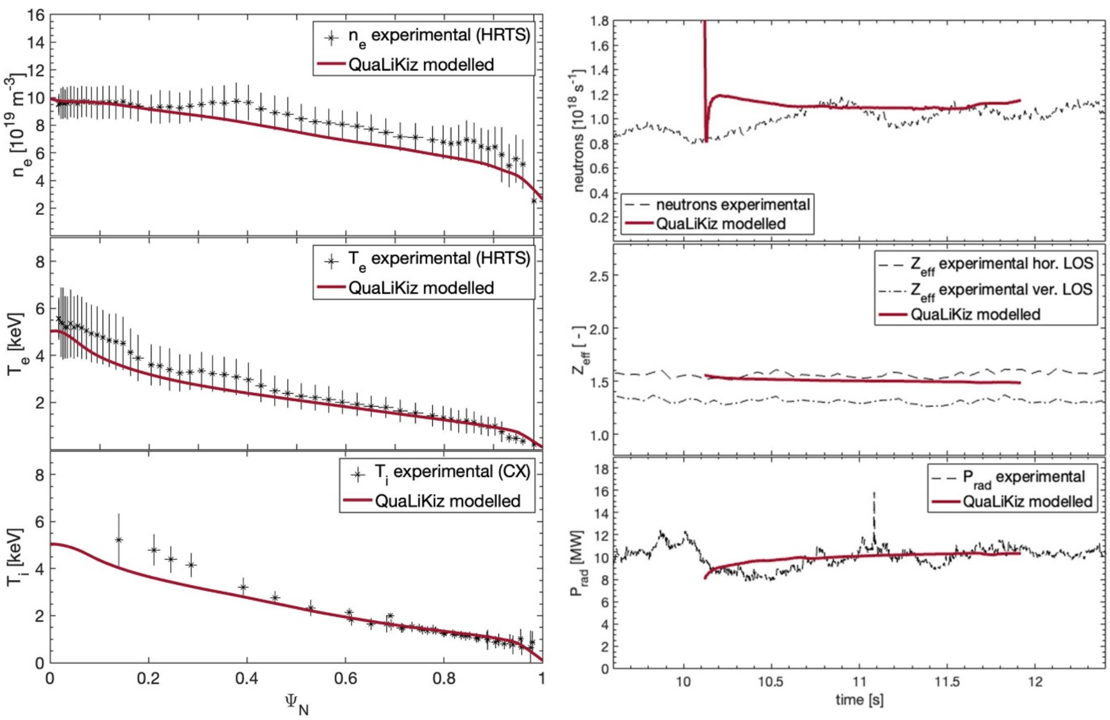

Figure 22. JINTRAC predictive modelling results for JPN 104663 with the QuaLiKiZ transport model. Left from top to bottom: electron density, electron and ion temperature. Right from top to bottom: neutron yield, Z_{eff} and radiated power. Modelling results (burgundy) are in reasonable agreement with the experiment.

Despite the fact that, in the JET baseline scenario, sustained (⩾5 s) high-current (⩾3.5 MA) and high D–T fusion (≈10 MW) performance proved incompatible in presence of a W divertor and with the power available in DTE2, sustained D–T plasmas were obtained at 3.0 MA in DTE3. However, because of the gas fuelling level required to maintain the compound ELM activity necessary for the stationarity of the pulse and the lack of optimization, the achieved fusion power was far from the record levels obtained in the hybrid and optimized fuel mix scenarios and somewhat lower than in the seeded JET ITER baseline scenario.

Finally, the scientific activity devoted to developing a high-current, high fusion performance scenario on JET has highlighted the need to develop modelling tools able to simulate the transport in the

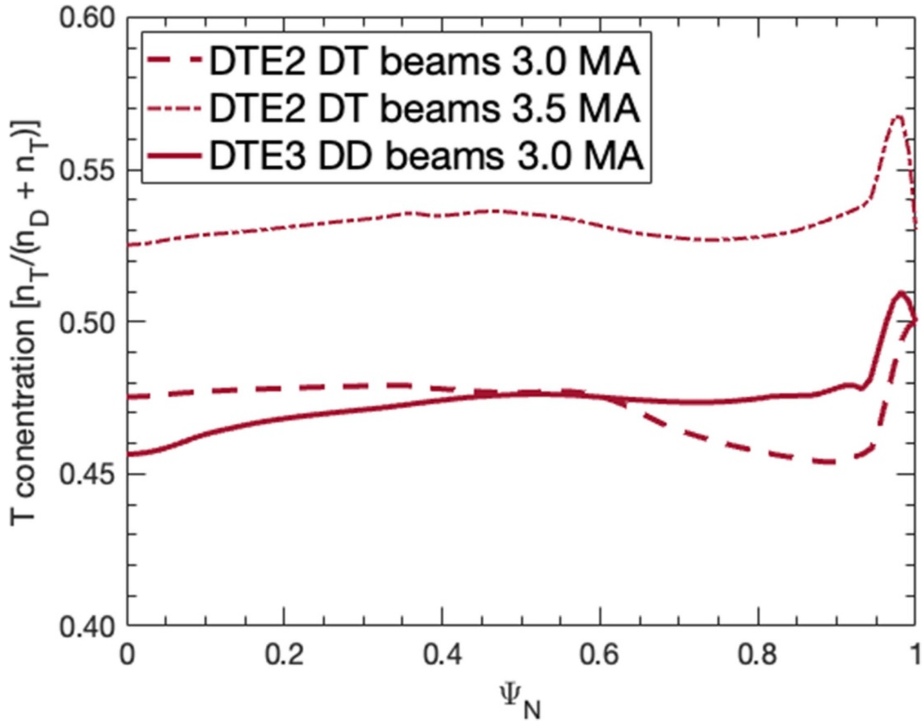

Figure 23. JINTRAC predictive modelling of the radial profile of the T concentration for the JET baseline scenario with 50–50 D–T NBI at 3.0 MA (JPN 99512) and 3.5 MA (JPN 99948), and with pure D NBI at 3.0 MA (JPN 104663).

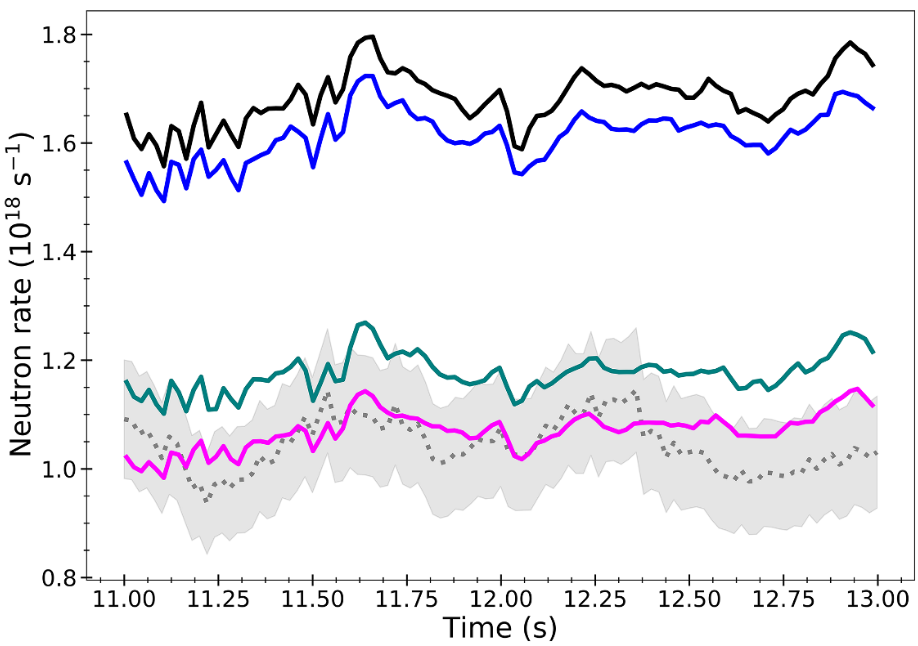

Figure 24. TRANSP neutron yield for JPN 104663: assuming a 50–50 D–T ratio and 2.5% Be concentration (black); assuming the D–T ratio predicted by JINTRAC and 2.5% Be concentration (blue); assuming the D–T ratio predicted by JINTRAC and 5.8% Be concentration, compatible with $Z_{\mathrm{eff}} \approx 1.8$ representing the upper margin of the measurement uncertainty (aqua) and assuming the D–T ratio predicted by JINTRAC, 5.8% Be concentration and an anomalous fast ion diffusivity of 2 $\mathrm{m}^2\,\mathrm{s}^{-1}$ (magenta). The experimental measurement is given by the dashed grey line and the uncertainty by the grey band. All effects (unbalanced D–T mix, increased plasma dilution and anomalous fast ion diffusivity) have to be invoked to explain the experimental measurement.

pedestal of an H-mode plasma, including the dependence on the isotope mass, and the difficulties inherent in running a high-current high Greenwald fraction ($\sim$0.8) pulse without enough auxiliary heating power. From this perspective, new data and further operational experience will have to be provided by next generation devices capable of producing D–T plasma and coming into operation before ITER, such as SPARC and BEST.

Acknowledgments

This work has been carried out within the framework of the EUROfusion Consortium, funded by the European Union via the Euratom Research and Training Programme (Grant Agreement No 101052200-EUROfusion). Views and opinions expressed are however those of the author(s) only and do not necessarily reflect those of the European Union or the European Commission or ITER. Neither the European Union nor the European Commission or ITER can be held responsible for them.

Data availability statement

The data cannot be made publicly available upon publication due to legal restrictions preventing unrestricted public distribution. The data that support the findings of this study are available upon reasonable request from the authors.

Author contributions

R Cicioni 0009-0005-8955-0192
Formal analysis (supporting)

N Grzybicka 0009-0009-2340-4474
Formal analysis (supporting)

E Peluso
Formal analysis (supporting)

References

[1] Loarte A *et al* 2025 *Plasma Phys. Control. Fusion* **67** 065023
[2] Creely A J *et al* 2020 *J. Plasma Phys.* **86** 865860502
[3] Maggi C F *et al* 2024 *Nucl. Fusion* **64** 112012
[4] Kappatou A *et al* 2025 *Plasma Phys. Control. Fusion* **67** 045039
[5] Garzotti L *et al* 2025 *Plasma Phys. Control. Fusion* **67** 075011
[6] Hobirk J *et al* 2023 *Nucl. Fusion* **63** 112001
[7] Rimini F G *et al* 2015 *Fus. Eng. Des.* **96-97** 165–70
[8] Kruezi U, Jachmich S, Koslowski H R, Lehnen M, Brezinsek S and Matthews G 2015 *Fus. Eng. Des.* **96-97** 286
[9] Nunes I *et al* 2014 Compatibility of high-performance operation with JET ILW *Proc. 25th IAEA Fusion Energy Conf., 3-18 October 2014* (St. Petersburg)
[10] Field A R *et al* 2021 *Plasma Phys. Control. Fusion* **63** 095013
[11] Frassinetti L *et al* 2021 *Nucl. Fusion* **61** 126054
[12] Lennholm M *et al* 2015 *Nucl. Fusion* **55** 063004
[13] Martin Y R *et al* 2008 *J. Phys. Conf. Ser.* **123** 012033
[14] Piron L *et al* 2025 *Plasma Phys. Control. Fusion* **67** 055006
[15] Predebon I, Hatch D R, Frassinetti L, Horvath L, Saarelma S, Chapman-Oplopoiou B, Görler T and Maggi C F 2023 *Nucl. Fusion* **63** 036010
[16] Birkenmeier G *et al* 2022 *Nucl. Fusion* **62** 086005
[17] Aiba N 2025 *Nucl. Fusion* **65** 082003
[18] Schneider P A *et al* 2023 *Nucl. Fusion* **63** 112010
[19] Saarelma S, Alfier A, Beurskens M N A, Coelho R, Koslowski H R, Liang Y and Nunes I 2009 *Plasma Phys. Control. Fusion* **51** 035001
[20] Frassinetti L *et al* 2023 *Nucl. Fusion* **63** 112009
[21] Nyström H *et al* 2025 Effect of diamagnetic flow stabilization on pedestal stability in JET and its importance for isotope mass effects *Proc. 51st European Physical Society Conf. on Plasma Physics* (Vilnius, Lithuania) 7 - 11 July 2025
[22] Zotta V K *et al* 2022 *Nucl. Fusion* **62** 076024
[23] Romanelli M *et al* 2014 *Plasma Fusion Res.* **9** 3403023
[24] Bourdelle C, Citrin J, Baiocchi B, Casati A, Cottier P, Garbet X and Imbeaux F 2015 *Plasma Phys. Control. Fusion* **58** 014036
[25] Houlberg W A, Shaing K C, Hirshman S P and Zarnstorff M C 1997 *Phys. Plasmas* **4** 3230
[26] Tamor S 1981 *J. Comput. Phys.* **40** 104
[27] Challis C D *et al* 1989 *Nucl. Fusion* **29** 563
[28] Eriksson L-G, Hellsten T and Willén U 1993 *Nucl. Fusion* **33** 1037
[29] Sertoli M, Carvalho P J, Giroud C and Menmuir S 2019 *J. Plasma Phys.* **85** 905850504

[30] Cenacchi G and Rulli M 1988 Upgrading of an equilibrium-transport Code for a multispecies free-boundary plasma *ENEA Report RTI/TIB(88)5*

[31] Maslov M *et al* 2023 *Nucl. Fusion* **63** 112002

[32] Hawryluk R J 1980 An Empirical Approach to Tokamak Transport *Physics of Plasmas Close to Thermonuclear Conditions* vol 1 ed B Coppi (CEC) p 19

[33] Lombardo J *et al* 2025 *Nucl. Fusion* **65** 096009